Chemical Engineering Journal 516 (2025) 163838

Contents lists available at ScienceDirect

Chemical Engineering Journal

journal homepage: www.elsevier.com/locate/cej

Targeting inflammatory macrophages with tailored bioactive β-glucan conjugated polymeric nanoparticles for the treatment of pancreatitis

Archana Karole [a], Yirivinti Hayagreeva Dinakar [a], Poonam Sagar [b], Shabi Parvez [a], Ravi Kumar [c], Shyam Lal Mudavath [c,*]

[a] Infectious Disease Biology Laboratory, Chemical Biology Unit, Institute of Nano Science and Technology, Knowledge City, Sector-81, Mohali 140306 Punjab, India
[b] Department of Food and Nutrition, National Agri-Food Biotechnology Institute, Knowledge City, Sector 81 Mohali, Punjab, India
[c] Department of Animal Biology, School of Life Sciences, University of Hyderabad, Prof. C.R. Rao Road, Gachibowli, Hyderabad 500046 Telangana, India

ARTICLE INFO

Keywords:
Acute pancreatitis
Chronic pancreatitis
PLGA nanoparticles
β-Glucan
Intestinal lymphatic system
Dectin-1 receptor

ABSTRACT

Macrophage (Mϕ) polarization plays vital role in inflammatory diseases, specifically M1 Mϕ worsens the disease by releasing pro-inflammatory cytokines. These M1 polarized Mϕ and intestinal M cells expresses Dectin-1 receptors, making it as potential target for treating inflammatory diseases such as Pancreatitis. Pancreatitis involves autodigestion of pancreatic tissue by activated trypsin enzyme, leading to severe inflammatory condition which affect major function of pancreas. Hence, the trypsin enzyme can be major trigger for enzyme-responsive drug delivery system. In this work, we developed enzyme-responsive, biocompatible, and orally administrable β-Glucan-conjugated PLGA nanoparticles (GNPs) targeting the Dectin-1 receptor for maximum accumulation at inflamed pancreas. We encapsulated and characterized Amlexanox (AMX)-loaded GNPs (AMX-GNPs), exhibiting significant drug loading content (DLC) 25%. The *in-vitro* studies revealed that AMX-GNPs release the drug in presence of trypsin enzyme. Further, it showed potential anti-inflammatory activity by modulating Mϕ polarization and reducing cytokine release from M1 polarized Mϕ. Additionally, we observed that GNPs follow the oral route and release the drug primarily in the inflamed pancreas via the intestinal lymphatic system (ILS). Preclinical studies confirmed that in acute and chronic pancreatitis animal models, AMX-GNPs effectively inhibit inflammatory cytokines, by regulating NF-κB activation pathways and M1 Mϕ polarization. Conclusively, AMX-GNPs showed promising potential for treatment of Pancreatitis due to trypsin mediated drug release, efficient binding and internalization through Dectin-1 receptor by active targeting of Mϕ polarization.

1. Introduction

Pancreatitis is a serious inflammatory disorder associated with the pancreas [1], caused by the overactivation of the trypsin enzyme. It is primarily classified as acute pancreatitis (AP) and chronic pancreatitis (CP), based on disease's progression and onset [2–4]. AP can be triggered by various factors, including gallstones, excessive alcohol intake, trauma, infection, drugs and genetic factor. In contrast, CP evolves as persistent pancreatic inflammation that eventually results in fibrosis and necrosis of glandular epithelium. This condition often caused by chronic alcohol consumption, persistent biliary dysfunction, cystic fibrosis, high blood glucose and various metabolic abnormalities[5].

Number of the pancreatitis cases are rising globally with approximately 10 to 45 cases per 100,000 people suffering from AP every year, while the prevalence of CP ranges from 50 to 200 cases per 100,000 people [6]. CP can cause irreversible damage to pancreatic tissue, which ultimately results in multiple organ dysfunction and possible transformation into pancreatic cancer [7]. The mortality rate in CP cases ranges from 20 % to 40 %, primarily associated with lack of targeted therapeutic option [8]. The inherent characteristics, anatomical position of the pancreas, and blood pancreas barrier are major hurdles for effective conventional drug delivery systems. The current treatments are administered intravenously , which is not only inconvenient but also non-targeted thus leading to unintended toxic effects [9]. Therefore, there is an urgent need to develop a targeted drug delivery system that can effectively reach the pancreatic microenvironment and potentially mitigate the inflammation in pancreas. Nowadays, nanomedicine has emerged as an effective and convenient drug delivery system for treatment of complex diseases. Here in this paper, we reported a nanoparticle mediated drug delivery system as an effective and promising therapeutic

* Corresponding author.
E-mail addresses: shyamlal_absls@uohyd.ac.in, shavs0502@gmail.com (S.L. Mudavath).

https://doi.org/10.1016/j.cej.2025.163838
Received 14 December 2024; Received in revised form 13 May 2025; Accepted 14 May 2025
Available online 16 May 2025

approach encapsulating hydrophobic drug (Amlexanox) in experimental animal model of L-arginine induced AP and CP disease model [10].

In this study, we designed patient friendly surface-modified nano drug carrier system for site-specific delivery of Amlexanox (AMX) to the inflamed pancreas, targeting both AP and CP diseases [3]. We reported that β-Glucan functionalized PLGA (Poly lactic-co-glycolic acid) nanoparticles loaded with AMX (AMX-GNPs) showed better therapeutic outcome for the treatment of pancreatitis. We achieved this notion by conjugating a yeast derived ligand 1,3 β-Glucan with PLGA through esterification. 1,3 β-Glucan is a bioactive, biocompatible and stable carbohydrate polysaccharide that exhibits biological response similar to innate immunity. It acts by activating phagocytic cells such as macrophages (Mϕ) and neutrophils, by binding to surface receptor (Dectin-1) on these cells. It is abundantly found in bacteria, yeast, plants, and exists in different structural configuration such as β-1,3-, 1,4- and 1,6-linked [11]. More specifically, baker's yeast has drawn considerable attention in recent five year for its known immunomodulatory effect due to 1,3 β-Glucan moieties. Additionally, it can be utilized as a bioactive carrier for targeted drug delivery [12,13]. It specifically binds to Dectin-1 receptors, which are expressed on intestinal M cells and Mϕ which plays a key role in immune responses such as macrophage polarization (M1 to M2 type Mϕ) at inflamed site [14–16]. Therefore, yeast derived β-Glucans can serve as effective ligand molecules for achieving therapeutic effect against inflammatory disorders. Additionally, we used PLGA, which is Food and Drug Administration (FDA) approved and widely recommended polymer for drug delivery, due to its high biocompatibility and biodegradable nature. PLGA has ability to effectively encapsulate hydrophobic and potent drug like AMX to enhance bioavailability [17–19].

Upon oral administration of AMX-GNPs, the β-Glucan functionalization protects the AMX-GNPs from the harsh acidic environment of the stomach. Once AMX-GNPs reach the intestine, they bind to Dectin-1 receptors on microfold cells (M cells) of Peyer's patches (PPs) and accumulate within intestinal lymphoid follicles, these follicles contain 80 % immune cells including Mϕ. These nanoparticles are then opsonized by Mϕ cells through Dectin-1 receptor, which further resulting in chemotactic behavior of immune cells and accumulating them at inflammatory site of pancreatic tissue. Further, the presence of elevated trypsin enzyme, facilitates the disassembly of AMX-GNPs by this enzyme, which cleaves the ester bond present in the AMX-GNPs and unload its cargo at the inflamed site. This targeted release is responsible for potential anti-inflammatory activity by inhibiting the Mϕ polarization to M1 and effectively converting them to M2 Mϕ. Thereby, causing the suppression of pro-inflammatory cytokines and simultaneous activation of anti-inflammatory cytokines [20,21].

We extensively characterized the GNPs by Fourier transform infrared (FT-IR), Nuclear magnetic resonance (NMR), UV-Visible spectroscopy, Dynamic light scattering(DLS), Transmission electron microscopy (TEM), Scanning electron microscopy (SEM), Atomic force microscopy (AFM) to confirm its size and drug encapsulation. We also examined the uptake ability and anti-inflammatory activity using cells-based assay. Additionally, we investigated *in-vivo* anti-inflammatory potential of AMX-GNPs in L-arginine induced pancreatitis model in Wistar rats. Further, we evaluated this notion on both acute and chronic pancreatitis experimental model and observed promising results. Our finding revealed that AMX-GNPs exhibits notable anti-inflammatory potential by downregulating the pro-inflammatory markers such as Tumor Necrosis Factor-α (TNF-α), Interleukin-1β (IL-1β), Interleukin-16 (IL-6) and regulating Nuclear Factor kappa B (NF-κB) activation pathways due to additive action of β-Glucan and AMX. Additionally, AMX-GNPs showed mitigation of pancreatic fibrosis, necrosis and other disease associated clinical symptoms in Wistar rats by balancing Mϕ polarization of the M1 phenotype toward an anti-inflammatory Mϕ, which ultimately suppressed the production of the inflammatory cytokines and nitric oxide synthase 2 (NOS2) expression. Our results suggested that efficacy of AMX-GNPs is very much promising, and it has significant translational potential due to patient compliance and safety profile. These can be employed as a therapeutic agent for clinical treatment of certain inflammatory disorders including AP and CP.

2. Materials and methods

2.1. Materials

Amlexanox (AMX) was purchased from Abcam USA, succinic anhydride, dicyclohexyl carbodiimide (DCC), DMF (Dimethylformamide), 4-dimethylaminopyridine (DMAP) and HOBt (1-Hydroxybenzotriazole) were procured from Tokyo Chemical Industry (TCI), PLGA (Poly (lactic-co-glycolic acid)), yeast derived β-1,3-Glucan that contain 1,6- Glucan side chain (molecular weight ~ 180 kDa), MTT (3-[4,5-dimethylthiazol-2-yl]-2,5 diphenyl tetrazolium bromide), Polyvinyl alcohol (PVA) and L-arginine monohydrochloride (L-arginine) were obtained from Sigma Aldrich.

2.2. Synthesis and characterization of β-Glucan conjugated polymeric nanoparticles (GNPs)

2.2.1. Synthesis of β-Glucan conjugated PLGA (βGlu-PLGA) through esterification reaction

Endotoxin free, baker's yeast (*Saccharomyces cerevisiae*) purified (98 %) β-Glucan was purchased from Sigma-Aldrich was used throughout study. In brief, a β-Glucan solution was prepared by dissolving 50 mg of β-Glucan in 2 mL deionized (DI) water, by vertexing for 5 min. Further resulting solution was sonicated for 5–10 min at 60℃ followed by addition of 100 μL of 1 N NaOH (sodium hydroxide) for complete dissolution. In the second step, 100 mg of PLGA was added in round bottom flask containing 20 mL of DMF and allowed to sonicate for 5 min. Then, 10 mg of DCC and 15 mg of HOBt was added to the solution and reaction mixture was stirred magnetically for 30 min at 0℃[22]. After 30 min, β-Glucan aqueous solution from first step was added, and stirring continuously until a clear solution was obtained. Next, 20 mg of DMAP was added into reaction mixture, which was then left for 24 h at room temperature. After the reaction was complete, EDC (N-(3-Dimethylaminopropyl)-N-ethylcarbodiimide) and DMAP impurity were removed through water extraction, the isolated product was purified via column chromatography. Finally, the reaction product was dried by lyophilization and stored at −20 °C.

2.2.2. Preparation of β-Glucan conjugated PLGA nanoparticles (GNPs)

To better understand the effects of surface-functionalized polymeric nanoparticles (GNPs) and plain polymeric nanoparticles (NPs), we prepared both GNPs and NPs nanoparticles. The single emulsion method is primarily used for the encapsulation of hydrophobic drugs in polymeric nanoparticles [23]. Therefore, we followed this method for nanoparticles development. First, nonaqueous phase was prepared by dissolving 20 mg of PLGA in 1 mL of DMSO followed by sonication for 10 min and stirring for 1 h. Subsequently, 10 mL of 1 % PVA was used as the aqueous phase. Further, nonaqueous phase was slowly transferred into the aqueous phase using a 5 mL syringe, and the reaction mixture was allowed to stir for overnight. The solution was then centrifuged at 14000 rpm (Revolution Per Minute) for 30 min at 4 °C. Resulting pellet was resuspended in DI water, and this process was repeated twice. To remove the remaining solvent, the nanoparticles were dialyzed for 24 h. After dialysis, nanoparticles were lyophilized and stored at 4 °C for long-term stability. Similarly, blank GNPs were also prepared using the same procedure[24].

2.3. Preparation of AMX-loaded GNPs (AMX-GNPs)

We dissolved βGlu-PLGA/PLGA and AMX in 10:1.5 ratio in DMSO and allowed the mixture to stir for 30 min. Then the mixture was transferred into 1 % PVA and incubated for 12 h at room temperature.

The hydrophobic interactions between βGlu-PLGA/PLGA part and AMX cause physical entrapment of AMX during βGlu-PLGA/PLGA due to its hydrophobic core [25]. The resulting solution was centrifuged at 14000 rpm for 30 min at 4 °C and dialyzed three time in DI water. Finally, the solution was lyophilized to obtain the dried formulation (AMX-GNPs/AMX-NPs), which was stored at 4 °C.

2.4. Characterization of AMX-loaded βGlu-PLGA nanoparticles (AMX-GNPs)

2.4.1. Attenuated total Reflectance-Fourier Transform Infrared (ATR-FTIR) spectroscopy

We performed ATR-FTIR spectroscopy (VERTEX 70v, Bruker FTIR spectrophotometer) to assess the conjugation of β-Glucan and PLGA (βGlu-PLGA), as well as the interaction between the drug and the nanocarrier. Each sample was scanned in the range of 400–4000 cm^{-1} with a resolution of 4 cm^{-1} and 64 scans [26].

2.4.2. ^1H NMR (Nuclear Magnetic Resonance) spectroscopy

For further confirmation of the ester bond linkage between β-Glucan and PLGA, reaction product was solubilized in deuterated DMSO (DMSO-d_6) at a concentration of 12 mg/mL. NMR Spectra were recorded using a Bruker Avance HD 400 MHz NMR spectrometer instrument [27].

2.5. Drug loading and encapsulation efficiency

The drug loading content (DLC) and drug encapsulation efficiency (DEE) of GNPs nanoparticles was assessed using a direct method using Ultraviolet (UV–Vis) Spectrophotometry analysis. In brief supernatant obtained after centrifugation of the AMX-GNPs was used to determine the concentration of free AMX. A calibration curve of AMX was plotted using its maximum absorption wavelength at 290 nm. The concentration of AMX in the supernatant and in GNPs nanoparticles was analysed using UV–Vis spectrophotometry at 290 nm. Percentage DLC and DEE was calculated using following equation: –

$$\textbf{Total drug encapsulated} = \text{Total drug added}\,(\mu g) - \text{Free drug}\,(\mu g)\,\text{in supernatant}$$

$$\textbf{Drug Loading Content}\ (\%) = \frac{\text{Encapsulated drug}\,(\mu g)\,\text{in NPs}}{\text{Total weight of polymer}\,(\mu g)} X100$$

$$\textbf{Drug Encapsulation Efficiency}\ (\%) = \frac{\text{Encapsulated drug}\,(\mu g)\,\text{in NPs}}{\text{Total drug}\,(\mu g)\,\text{added}} \text{X}\,100$$

2.6. X-ray powder diffraction (PXRD) analysis

A diffractogram of powder AMX, β-Glucan (βGlu), PLGA, β-Glucan PLGA conjugate (βGlu-PLGA), AMX-GNPs and Blank GNPs was acquired to ascertain the diffraction patterns of sample using X-ray powder diffractometer (Bruker, Advance D-8 Diffractometer) instrument. The diffraction patterns were recorded over a 2θ range of 10–70° at a scanning rate of 50 scans/min.

2.7. Size and morphology of nanoparticles

To assess the hydrodynamic diameter, surface charge and polydispersity index (PDI) of nanoparticles using a Two Angle Particle size analysis (DLS; Dynamic light scattering), Malvern Zetasizer Nano ZS instrument (ZEN5600 Model, UK). The particle size and PDI were measured at a detection angle of 90°, while at zeta potential was measured at 120°. In brief, the samples were diluted with distilled water in a 1:100 ratio and transferred into disposable sample cuvette (polystyrene cuvette; DTS0012; Malvern). Analysis was conducted in triplicate, and the mean of three individual values represented as the hydrodynamic size, PDI and zeta potential. To further ascertain the size and surface morphology of nanoparticles, we performed electron microscopy using TEM (Transmission electron microscopy; JEM-2100 Plus JEOL), SEM (Scanning electron microscopy: JSM-7610F Plus JEOL) and AFM (Atomic force microscopy; Bruker multimode 8, NanoScope 9.1). For TEM analysis, samples were diluted in DI water and drop casted onto a carbon-coated copper grid (Ted Pella Inc, # 300 mesh size). Similarly, for AFM and SEM analysis, a silicon wafer was used as the substrate. All images were captured at different resolutions and processed using the respective camera software. To predict the possible biological behavior, we conducted stability studies of nanoparticles upto five days in 7.4 pH PBS buffer and 10 % DMEM media at 37 °C (detailed procedure is provided in **Supplementary File**).

2.8. In vitro drug release study

The percentage of AMX release from the nanoparticles was evaluated in different physiological pH condition, both in presence and absence of trypsin enzyme. The dispersion of AMX-GNPs and AMX-NPs (1 mg/mL AMX) respectively, was prepared in phosphate buffer saline (PBS) at pH values of 1.2 and 7.4. The nanoparticle dispersions were transferred into dialysis bag (Thermo Fisher with cutoff molecular weight ~ 10 kDa) and securely clipped at both ends. Further these bags were immersed into 250 mL of buffer solution containing 1 % tween-80. At initial 2 h of interval, we performed dialysis in PBS at pH 1.2. Subsequently, the dialysis bags were transferred to a pH 7.4 buffer solution. At this point, trypsin enzyme (100 IU) was added, and system was stirred at 80 rpm at 37 °C. At predetermined time intervals, 1 mL of the sample was collected, and an equal volume of fresh medium was added to maintain the total volume. The concentration of released AMX was determined using UV–Vis spectroscopy at a wavelength of 290 nm[20].

2.9. In vitro cell culture study

RAW264.7 (murine macrophage cell line), Caco-2 (human colorectal adenocarcinoma cells) and Raji B (human B lymphoblastoid cell) cells were purchased from National Centre for Cell Science Pune, India. Caco-2 cells were cultured in high glucose Dulbecco's modified eagle medium (DMEM) with 15 % fetal bovine serum (FBS), along with 1 % Penicillin-streptomycin. Similarly, RAW264.7 and Raji B cells were cultured in 10 % Fetal bovine serum containing complete media. Cells were incubated at 37 °C in humidified atmosphere of 5 % CO_2.

2.10. Cell cytotoxicity assay

To assess the safe concentration of free drug and nanoparticles, MTT assay was performed on L929, Caco-2 and RAW264.7 cells. In short, cells were seeded at density of 50,000 cells/well in cell culture treated 96-well plates and incubated for 24 h at 37 °C in humidified atmosphere of 5 % CO_2. After incubation, the cells were treated with different concentration of free AMX, βGlu, AMX-NPs and AMX-GNPs. Concentration ranging from 10 to 120 μg/mL prepared in complete media and cells were incubated for additional 24 h. A PBS treated cells were used as control group. Following treatment schedule, media was replaced with 100 μL of MTT reagent and allowed to incubate for 4 h at 37 °C. Then, DMSO (100 μl) was added to each well to dissolve the formazan crystals. The absorbance was measured at 570 nm using a microplate reader (Tecan). Each experiment was conducted in triplicate to ensure reproducibility.

To further confirm the safe concentration of nanoparticles (at which cell viability was found to be above 90 %), we carried out qualitative analysis using LIVE/DEAD cell assay. Briefly, RAW264.7 cells were seeded into a 96-well plate with cell number 40,000 cells/well. After 24 h incubation, cells received treatment with free drug (AMX), βGlu, Blank NPs and GNPs, AMX-GNPs and AMX-NPs at concentration of 50 μg/mL

and incubated again for 24 h. The cells containing only culture media, used as negative control, while cells treated with 1 % triton-X 100 were used as positive control. Subsequently, LIVE/DEAD cell staining was performed with phenol red free DMEM media, followed by PBS wash. Stained cells were examined using an inverted fluorescence microscope (Invitrogen™ EVOS™ M5000 Cell Imaging System).

2.11. Cellular uptake

Fluorescein or FITC-loaded NPs (NPs) and FITC-loaded GNPs (GNPs) were synthesized to investigate cellular drug uptake *in vitro*. To determine cell-specific nanoparticles uptake, drug uptake studies were conducted on macrophages (RAW264.7) and fibroblast (L929) cells lines.

The internalization of GNPs by pro-inflammatory macrophages (Mϕ) was analyzed both qualitatively and quantitatively. For the qualitative analysis (fluorescence-based), RAW264.7 cells were seeded into glass bottom confocal dish (Nunc Glass Bottom Dish, Thermo scientific) at a cell density of 60,000 cells/mL. After 24 h incubation, cells were washed with 1X-PBS, and M1 Mϕ polarization was initiated by incubating cells with 100 ng/mL of Lipopolysaccharide (LPS) in cultured medium (without FBS) for 12 h. Further, the cells were washed three times with PBS and then treated with NPs or GNPs in culture media. Following 4 h incubation, treated cells were received wash with ice cold PBS, fixed with 4 % paraformaldehyde for 10 min. Fixed cells were stained with Rhodamine/phalloidin and Hoechst 33,342 stain for 30 and 5 min, respectively, to visualize the cytoskeleton and nucleus of cells[28]. All samples were analysed by an inverted fluorescence microscopy (Leica Laser microscope; DMi8). Similarly, to determine nanoparticle uptake in non-inflammatory cell types, the same procedure was carried out with L929 cells (without LPS).

Subsequently, SEM-based cellular uptake analysis was also performed to confirm nanoparticle uptake in Mϕ, with detailed protocol is provided with **Supplementary File**.

Quantitative estimation was performed using flow cytometry in M1 polarized Mϕ. In brief, RAW264.7 Mϕ cells were cultured in a 6-well plate at the cell number 60,000 cells/well. After 12 h of incubation, LPS (100 ng/mL) was added to induce M1 polarization in RAW264.7 cells. Followed by treatment with nanoparticles, cells received four washes with cold PBS. At the end, cells were kept suspended in 200 μL PBS to avoid cells drying and then scraped from the bottom of the well by scraper. All samples were further analyzed using a Flow cytometer (BD FACS Aria).

2.12. Assessment of in vitro anti-inflammatory activity

To find anti-inflammatory potential nanoparticles against pancreatitis, we checked the level of key pro-inflammatory cytokines and nitrite levels. Briefly, M1 polarized (LPS-activated) macrophages (Mϕ) were incubated with different treatment groups (bGlu, AMX and AMX-GNPs) for 24 h. Subsequently, nitrite levels in supernatant were assessed using the Griess reagent. Each supernatant sample was mixed with an equal volume of modified Griess reagent. After a 15 min incubation with reagent, absorbance was measured at 540 nm, and NO_2^- concentrations were determined using a sodium nitrite standard curve.

The supernatant from the same sample was then used to quantify the levels of IL-1β, TNF-α, and IL-6 (pro-inflammatory cytokines). To calculate unknown concentration of cytokines, ELISA (Enzyme Linked Immunosorbent Assay) was performed, following the protocol provided by the manufacturer (Mouse ELISA Kit, Abcam). The concentrations were calculated based on standard curves provided with ELISA kits.

2.13. Macrophage polarization study

2.13.1. Immunofluorescent staining of polarized macrophages

RAW 264.7 cells were cultured in glass bottom confocal dishes at a density of 50,000 cells/mL and incubating for 24 h at 37 °C in a humidified atmosphere with 5 % CO_2. To induce M1 Mϕ polarization, cells were treated with LPS (100 ng/mL), while for M2 Mϕ polarization, cells were treated with IL-4 (20 ng/mL) for 24 h. After washing with PBS, 1 mL of fresh culture media (without FBS) containing 50 μg/mL of βGlu/AMX/AMX-GNPs was added to the dishes. Following a 24 h treatment period, the fixed M1 and M2 polarized Mϕ were stained with TRITC-labeled CD80 antibody (Invitrogen, USA) and FITC-labeled CD163 antibody (Invitrogen, USA), respectively. The effects of treatment on Mϕ polarization were then observed using a confocal laser microscope.

2.13.2. Flow cytometric analysis

For quantitative analysis, flow cytometric analysis was performed. In brief, RAW 264.7 cells were plated in a 6 well culture plate at concentration of 50,000 cells/mL in 10 % FBS containing DMEM medium. The plate was then placed at 37 °C in 5 % CO_2 incubator for 24 h. M1-type Mϕ differentiation was carried out using 100 ng/mL LPS, while M2-type Mϕ differentiation was carried out with 20 ng/mL IL-4. Then culture media in the 6-well plate was then replaced with fresh media (without FBS) that contained 50 μg/mL of βGlu/AMX/AMX-GNPs. After 24 h incubation, PBS wash was given to cells and scraped from the plate. The cells were stained with CD11b-FITC, F4/80-PE/Cy7, CD80-APC, CD86-PE, CD163-PE, CD206-APC (Invitrogen, USA) at room temperature for 30 min, followed by centrifugation. Further, cells were washed and resuspended in 200 μL of PBS. Cells sorting was performed with BD flow cytometer and data was analysed using FlowJo software.

2.14. Establishment of M cell model and co-localization study

As we hypothesized the internalization of GNPs might takes place through M cells. To test this notion, we developed a co-cultured Caco-2 and Raji B cells-based intestinal M cell model that can mimic nanoparticles transportation across the small intestinal epithelial barrier. The detailed study protocol is explained in **Supplementary File**. Briefly, the apical compartments of *trans*-well plate were incubated with FITC-loaded NPs/GNPs in 15 % DMEM high glucose medium. After 12 h of incubation, sample were collected from both apical and basolateral part. Further, the fluorescence intensity of FITC-loaded nanoparticles was then measured using multimode plate reader excitation 495 nm and emission at 519 nm.

2.15. Animal study

All preclinical studies were performed on Wistar rats. Animal experiment was conducted accordance with Committee for Purpose of Control and Supervision of Experimental Animals (CPCSEA). 7–8 weeks old, Male/Female Wistar rats with 220–300 gm body weight were procured from the National Institute of Pharmaceutical Education and Research (NIPER), Mohali, Central Animal Facility (CAF). The Wistar rats were housed in central facility for animal at Indian institute of science education and research (IISER Mohali, India). Animals were provided with free rodent pellet diet and water ad libitum. The experiment protocols were approved by Institutional Animal Ethics Committee (IAEC) IISER Mohali, accredited by CPCSEA. The approval project number is IISERM/SAFE/PRT/2021/021.

2.15.1. Assessment of in vivo safety profile

An *in vivo* oral acute toxicity study was performed to assess the safety profile of nanoparticles in biological system. In brief, Wistar rats were randomly divided into two group; control and AMX-GNPs treated group, and seven animals (n = 7) were kept in each group.

Treatment schedule

Group 1. (Normal control): Received only saline by oral gavage for fourteen days.

Group 2. (AMX-GNPs treated group): Received AMX-GNPs (100

mg/kg equivalent dose of AMX) formulation was orally given for fourteen days.

Body weight, health condition and onset sign of toxicity was continuously observed during the treatment schedule. At the end of experiment, rats were sacrificed, and all vital organs were aseptically excised. Then, the tissue sample were fixed in formalin fixation solution for histological analysis and hematoxylin and eosin (H&E) staining was performed. Alterations in biochemical parameters were analysed using blood and urine samples.

2.15.2. Biodistribution of nanoparticles

To understand the biodistribution of nanoparticles after oral administration, we performed an *in vivo* biodistribution study in diseased rats. For this we utilized fluorescent dye indocyanine green (ICG) dye, which is non-toxic and widely used for tracking biodistribution molecules. Therefore, we synthesized ICG-tagged NPs (NPs) and ICG-tagged GNPs (GNPs) in study. ICG-tagged nanoparticles were developed using the single emulsion method, ICG is hydrophobic dye that can be loaded in polymeric nanoparticles similar to AMX. We followed modified protocol from [29], for the preparation of ICG loaded GNPs which follows similar protocol as preparation of AMX-loaded GNPs/NPs. Here, instead of encapsulating the drug (AMX), we encapsulated ICG into the polymeric nanoparticles. We used dye: polymer ratio 1:10 (w/w) and removed the unencapsulated ICG by dialysis bag (cut-off mol wt. ~ 3.5 kDa). The encapsulated GNPs were further used for the biodistribution study.

Furthermore, we randomly divided animals into three groups (n = 3, each group). The rats were fasted overnight, and then received oral treatment of NPs or GNPs (5 mg/kg) in assigned group and saline treated group was used as untreated control group. After dosing, rats were sacrificed at predetermined time point. Gastrointestinal and all vital organs, PPs, pancreas and mesenteric lymph node (MLN) were isolated for in-vivo imaging system (IVIS) analysis. *Ex vivo* IVIS imaging was performed using a Perkin Elmer IVIS system with an excitation/emission filter of 720–780 nm/ 830–890 nm.

2.15.3. Route of drug transportation

ILS-mediated drug delivery of GNPs after oral administration was investigated using an earlier optimized *in situ* loop formation assay [30]. In short, Wistar rats were divided into two groups, with each group containing three animals. One group received only saline, were served as untreated control (without inhibitor). While second group was initially treated with an intraperitoneal injection of 3 mg/kg cycloheximide, which is commonly used as an intestinal lymphatic blocker [31]. After 1 h of cycloheximide dosing, Wistar rats were anesthetized using of E-Z 7000 Classic Anesthesia System. An intestinal loop was formed between the duodenal and ileal ends of the small intestine using silk sutures, ensuring the mesenteric system remained intact. ICG-tagged GNPs (GNPs) were incubated in the loop segment and allowed to be absorbed for 2 h within the body cavity. After incubation period, intestinal segment was isolated from the animal. Subsequently, PPs, intestinal villi and lymphatic vessels were separated from the segment. Further, fluorescence signal of lymphatic vessels was analysed using IVIS imaging system. PPs and intestinal villi were stored in 4 % paraformaldehyde (PFA) solution, followed by sucrose processing, cryosectioning was performed. To determine role of M cells in PPs mediated internalization of GNPs, immunofluorescence staining was carried out on sections of PPs and villi. Tissue sections were stained with a primary GP-2 monoclonal antibody (Cloud clone, USA; 1:100) for 2 h at room temperature. After that, TRITC-tagged secondary antibody (Cloud clone, USA: 1:200) was used for fluorescence detection. M cell mediated colocalization of GNPs was examined using a confocal laser scanning microscopy.

2.15.4. Therapeutic efficacy against acute pancreatitis

The acute pancreatitis (AP) disease model was used to assess the anti-inflammatory potential of GNPs in acute conditions. Here, we used L-arginine for induction of AP in Wistar rats [32]. Overall, AP model was developed in overnight fasted Wistar rats. All test animals received two high intraperitoneal doses of L-arginine (2.5 gm/kg in saline) at one-hour interval. Disease development was confirmed by analysing serum amylase and lipase level. Animals confirmed with AP were then distributed into five distinct groups. Further, drug treatment was initiated 24 h after disease induction. The treatment group included free Amlexanox (AMX), β-Glucan (βGlu) and AMX-GNPs, all administered orally at a dose of 100 mg/kg of body weight. The dosing schedule was carried out at 24 h and 48 h of post L-arginine treatment and change in body weight of animal was also noted. After 24 h of dosing, blood samples were withdrawn, and animals were euthanized.

Dosing schedule

Group 1 (**Healthy control**; n = 5): Wistar rats received distilled water *p.o.* (per oral).

Group 2 (**AP model/disease group**; n = 6): Wistar rats were injected intraperitoneally with L-arginine (2.5 gm/kg, 2X dose at 1 h interval).

Group 3 (**βGlu**; L-arginine + βGlu; n = 6): Disease animals received treatment of β-Glucan [100 mg/kg/*p.o*].

Group 4 (**AMX**; L-arginine + AMX; n = 6): Disease animals received treatment of Amlexanox [100 mg/kg/*p.o*].

Group 5 (**AMX-GNPs**; L-arginine + AMX-GNPs; n = 6): Disease animals received treatment of AMX-GNPs formulation [100 mg/kg/*p.o*].

At the endpoint (72 h post-induction), organs were harvested, and pancreases were weighed. Isolated tissues were fixed in 10 % formalin solution for 24 h and were further processed for histological staining (H&E, Trichrome staining) and Immunohistochemistry (IHC) observations. The *in-vivo* anti-inflammatory activity against the AP model was assessed through H&E, trichrome staining, immunohistochemistry, immunofluorescence and Real-time polymerase chain reaction (RT-PCR) studies. Detailed protocols were mentioned in **Supplementary File.**

2.15.5. Therapeutic efficacy against chronic pancreatitis

An experimental animal model of chronic pancreatitis (CP) was also established to assess the long-term anti-inflammatory potential of AMX-GNPs against chronic condition. Similar to AP model, L-arginine was used to induce CP in Wistar rats. We have developed the CP model with some modification in already exciting protocol [33]. Disease model was established in three phases- 1st high dose (induction of inflammation), 2nd medium dose (70–80 % damage in acinar cell) and 3rd high dose (necrosis). In brief, on day zero, overnight fasted test animal received two intraperitoneal injections of L-arginine at dose of 2.5 gm/kg in one-hour interval. Subsequently, a medium dose of L-arginine (3.5 gm/kg) was injected intraperitoneally on day 2, 4, 6, 8, 10, 14, 18, 22 and day 26. At the end, higher dose of L-arginine (2.5 gm/kg, *i.p.,* two consecutive doses, at 1 h apart) was administered to the animals. To confirm the disease development, serum amylase and lipase levels were measured along with monitoring body weight of the animals. Disease animals were randomly distributed into five distinct groups. Further, three group of rats were orally received different treatment of free Amlexanox (AMX), β-Glucan (βGlu) and AMX-GNPs at dose of 100 mg/kg, *p.o* respectively. The dosing schedule was followed every alternate day for upto four weeks to find long term therapeutic effects of treatments. Change in body weight and overall health of animal was also noted. After 24 h of dosing completion, blood samples were withdrawn, and animals were euthanized.

Dosing schedule

Group 1 (**Healthy control**; n = 5): Wistar rats received distilled water *p.o.* (per oral).

Group 2 (**CP model/disease group**; n = 10): Wistar rats received multiple doses of *i.p.* L-arginine.

Group 3 (**βGlu**; L-arginine + βGlu; n = 6): Disease animal received

treatment of β-Glucan [100 mg/kg/*p.o.*].

Group 4 (**AMX**; L-arginine + AMX; n = 6): Disease animal received treatment of Amlexanox [[100 mg/kg/*p.o.*].

Group 5 (**AMX-GNPs**; L-arginine HCl + AMX-GNPs; n = 6): Disease animal received treatment of AMX-GNPs formulation [100 mg/kg/*p.o.*].

At the endpoint, organs were harvested, and pancreas weights were noted. The isolated tissues were fixed in 10 % formalin solution for 24 h and were further used for histological and Immunohistochemical analysis. *In vivo* anti-inflammatory potential of different treatment against the CP model was assessed using H&E, Trichrome staining, immunohistochemistry, immunofluorescence and gene expression studies. This detailed protocol was given in the **Supplementary File.**

3. Results and discussion

3.1. Synthesis and Characterization of β-Glucan conjugated PLGA (βGlu-PLGA)

PLGA is a safe, biocompatible and biodegradable polymer and known for its use as carrier in drug delivery. Moreover, it allows surface modification with different ligands and antibodies enabling active targeting for the treatment of numerous diseases[19,34,35]. Owing to that, we conjugated PLGA with β-Glucan. Specifically, we used baker's yeast derived natural polysaccharide (1,3 β-Glucan) due to its known biomimetic effect and biocompatible nature[36]. The synthesis of βGlu-PLGA was carried out through a modified esterification reaction procedure. The reaction steps are shown in the following schematic illustration, mentioned in Fig. 1C. We conjugated PLGA with β-Glucan, and successful conjugation was confirmed by FTIR and NMR spectroscopy.

PLGA showed characteristic peak of −C=O, −C-O-C, –CH- functional group in FTIR spectra at wavelength of 1755 cm^{-1}, 1086 cm^{-1} and 2996–2949 cm^{-1}, respectively (Fig. 1A). Further, characteristics peaks for free β-Glucan (βGlu) were observed at 3347 cm^{-1} for –OH (broad peak) stretch and 1036 cm^{-1} for −C-O-C stretch. In βGlu-PLGA conjugate, we observed, shifting in carbonyl peak (from 1755 to 1778 cm^{-1}) due to ester bond formation between a β-Glucan and PLGA. Additionally, presence of characteristics peak at 3347 cm^{-1} and 1086 cm^{-1} that correspond to –OH (β-Glucan) and −C=O group (Fig. 1A), represents conjugation between PLGA and β-Glucan. To further confirm the conjugation, we characterized reaction product (βGlu-PLGA) using ^{1}H NMR spectroscopy. The ^{1}H NMR spectrum of βGlu-PLGA product (Fig. 1B) showed characteristic proton peaks at $\delta = 1.47$ ppm for $–CH_3$, $\delta = 4.30$ ppm for $–CH_2$-O, $\delta = 4.42$ ppm for –OH, $\delta = 4.42$ ppm for $–CH_2$-CH_3, $\delta = 5.60$ ppm due to −O=C-O of PLGA. Further the β-Glucan showed peaks at $\delta = 2.88$ ppm due to Ar-CH, $\delta = 3.50$ ppm and 3.82 ppm for aliphatic-OH, Ar-OH showed $\delta = 5.20$ ppm and 4.8 ppm, $\delta = 7.96$ ppm of –CH and (−C-O-O). The presence of these characteristic peaks in ^{1}H NMR spectrum of the final product confirms the successful conjugation between β-Glucan and PLGA.

3.2. Preparation and characterization of nanoparticles

PLGA or βGlu-PLGA nanoparticles were prepared using single solvent emulsification method [23], as depicted in Fig. 1D. For comparison, we synthesized both AMX-GNPs and AMX-NPs. Initially, the hydrodynamic size of AMX-NPs and AMX-GNPs was measured using a DLS. We observed hydrodynamic diameters for AMX-NPs and AMX-GNPs to be around 183.4 ± 11.5 nm and 228.6 ± 07.8 nm, respectively, as depicted in Fig. 1E. We also assessed polydispersity index (PDI) of nanoparticles, which were observed at 0.207 ± 0.01 for AMX-NPs and 0.194 ± 0.02 for AMX-GNPs (Table 1), strongly represents that the particles were monodispersed. The increase in the size of AMX-GNPs compared to AMX-NPs was observed, which attributed to the conjugation of β-Glucan to PLGA nanoparticles.

Further, the zeta potential of nanoformulation was measured and observed to be −19.7 ± 3.10 for AMX-NPs and –22 ± 1.80 mV for AMX-GNPs (Fig. 1F), which means the nanoparticles have extreme negative surface charge and it can prevent the aggregation between the nanoparticles. We also characterized the particle size, shape and surface morphology of nanoparticles using TEM, SEM and AFM.

TEM analysis (Fig. 1G) revealed that AMX-GNPs were in nano size range 100–120 nm. This observed size was corroborated with observations in SEM and AFM analysis, which showed nanoparticles size ranging from 100-130 nm (Fig. 1H&I).

The stability of nanoparticles is primary concern and important parameter for long term storage of the formulation, as it affects their biological stability and distribution. Therefore, to predict the possible biological behavior, we conducted stability studies of AMX-GNPs nanoparticles for five days in 7.4 pH PBS buffer and 10 % DMEM media at 37 °C (depicted in **supplementary file**, Fig. S1D&E). After analysing change in particle size and PDI value, we found no significant changes in either PBS or DMEM media. This is possibly due to negative surface charge and the presence of a polysaccharide moiety on nanoparticle surface. These results confirmed that AMX-GNPs have good colloidal stability.

3.3. Drug loading and release studies

The drug release was quantified by using calibration curve for AMX, which showed maximum absorbance at 290 nm (Fig. S1A, **Supporting information**). In this work, NPs and GNPs were used as nanocarrier for the delivery of hydrophobic drug AMX [37]. The AMX was encapsulated into GNPs and NPs using a single solvent emulsion method [23]. briefly, the drug was loaded into non-aqueous phase at the time of formulation preparation. The percentage DLC, DEE of AMX was quantitatively estimated by using UV analysis. The % AMX loading was found to be 23.5 % in NPs formulation and 25 % in GNPs formulation, which indicates that β-Glucan conjugation did not affects the drug loading (Table 1). The optimal DEE was calculated to be around 88 % for AMX-NPs and 90 % for AMX-GNPs formulation (shown, in Table 1), which is consistent with earlier studies on PLGA based nanoparticles [38].

Additionally, powder X-ray diffraction (XRD) analysis was performed to examine change in diffraction pattern of AMX after incorporation in the GNPs formulation with other formulation components affects the crystallinity of the drug after encapsulation in nanoparticles. AMX alone showed crystalline nature in XRD spectra by exhibiting sharp peaks in diffractogram. However, after incorporation of the AMX into GNPs, the peak intensity was reduced in AMX-GNPs/NPs. That suggests, crystallinity of AMX was reduced and leads to conversion into an amorphous state within GNPs formulation (Fig. S1B, **Supporting information**).

Further, ATR-FTIR spectroscopical analysis was carried out to understand the interaction between AMX, NPs and GNPs components. In FTIR spectrum (Fig. S1C, **Supporting information**) the presence of functional groups and related characteristic peaks of AMX in both AMX-GNPs and AMX-NPs, whereas these peaks were absent in blank NPs. Which further confirms that AMX was successfully loaded inside the GNPs core (Fig. S1C, **Supporting information**).

The primary notion behind developing AMX-GNPs was to achieve targeted drug delivery after oral administration. However, it totally relies upon the drug release profile at specific pH and microenvironment of GIT. As proteolytic enzymes are observed to be overexpressed in pancreatitis condition, so in this case we focused on trypsin enzyme. That can cleave ester bond in AMX-GNPs and facilitate drug release at inflamed site only[39]. To assess the drug release profile, we compared AMX release under normal and acidic condition, with presence or absence of trypsin enzyme (Fig. 1J). The enzyme was added in releasing media after two hours of the initial time point. We observed that AMX exhibits extensive release (upto 60 %) from AMX-NPs (without β-Glucan coating) in acidic condition (pH 1.2) within 2 h, likely due to instability of AMX-NPs in acidic environment (Fig. 1J). Further, this pattern continued in presence of trypsin enzyme. Whereas, AMX-GNPs showed

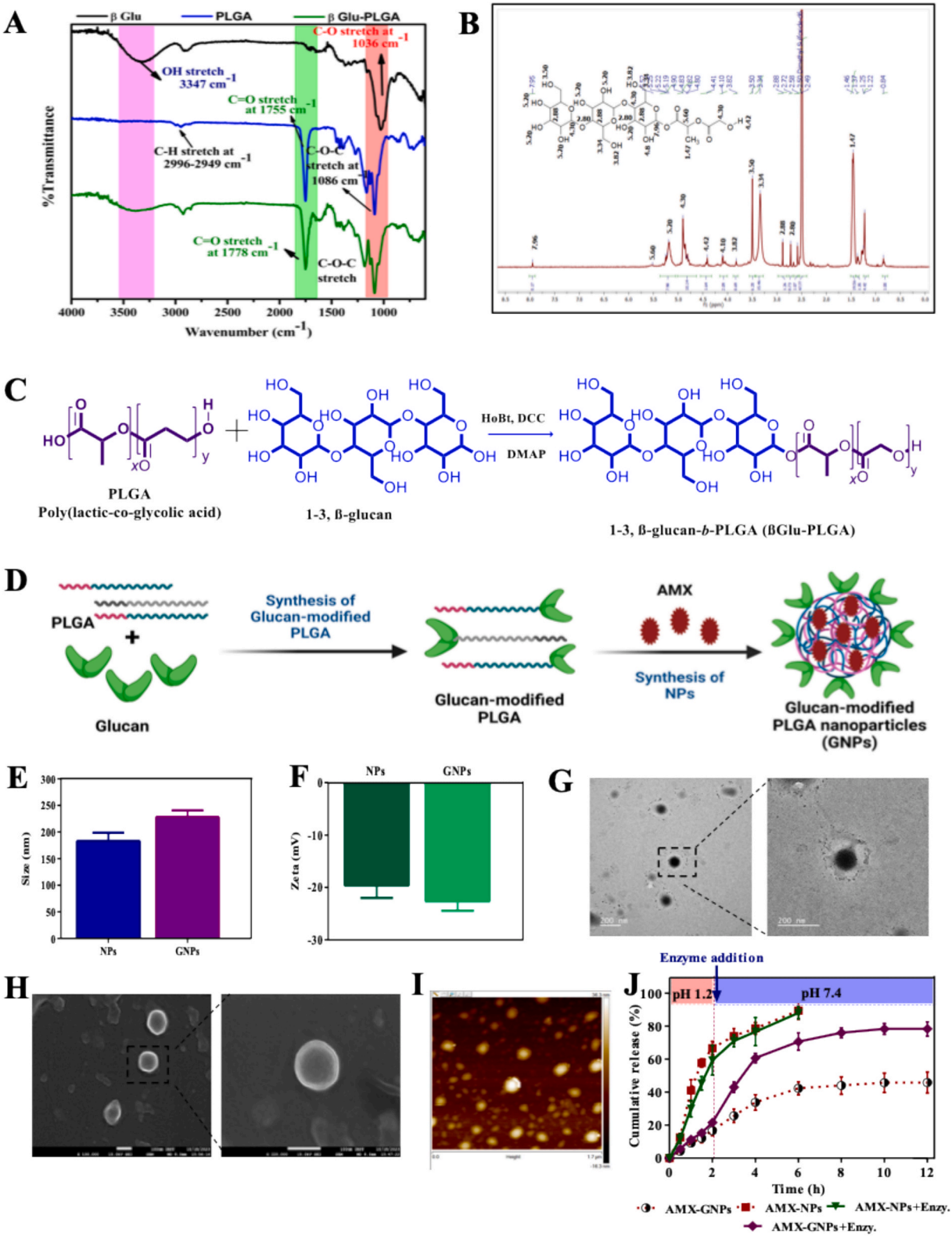

Fig. 1. Schematic and graphical representation for synthesis and characterization of βGlu-PLGA conjugate. (A) FTIR spectra of PLGA, β-Glucan (βGlu) and βGlu-PLGA conjugate product. (B) ^{1}H NMR spectrum of conjugate product (βGlu-PLGA). (C) Schematic representation of βGlu-PLGA synthesis and characterization of NPs and GNPs. (D) Pictorial representation of steps involved in GNPs nanoformulation. (E&F) Hydrodynamic diameter and surface charge of NPs and GNPs (G). TEM characterization of GNPs with extended view in right image depicts size ranging from 100-120 nm (H). SEM characterization of GNPs with zoomed view H' shows spherical nanoparticle size ranging from 100-120 nm (I). AFM characterization of the of GNPs nanoparticles depicted in AFM image showed size in 100–130 nm. (J). *In vitro* AMX release profile of AMX-loaded GNPs/NPs formulation at 1.2 pH and 7.4 pH, with and without trypsin enzyme (Enzy). All values are presented as means ± SEM (n = 3).

Table 1
Tabular representation of the hydrodynamic size, polydispersity index, zeta potential, percentage DLC and DEE values of AMX-loaded PLGA nanoparticles (AMX-NPs) and AMX- loaded βGlu-PLGA Nanoparticles (AMX-GNPs).

Formulation name	Hydrodynamic Size (nm)	PDI	Zeta potential (mV)	% DLC	% DEE
AMX-NPs	183.4 ± 11.5	0.207 ± 0.01	−19.7 ± 3.10	23.5 %	88 %
AMX-GNPs	228.6 ± 07.8	0.194 ± 0.02	–22.0 ± 1.80	25.0 %	90 %

minimal drug release under acidic condition, with only 18–20 % AMX released in the first 2 h, owing to acid-resistant coating of β-Glucan over nanoparticles surface. Further in intestinal pH (7.4), AMX-GNPs showed a sustained drug release pattern over next 24 h with a total 40 % drug release [36]. While, in presence of the trypsin enzyme, AMX-GNPs showed triggered release (upto 80 %) between 12 h interval, which is significantly improved as compared to without trypsin. Here, AMX effectively released in surrounding medium after the enzyme mediated cleavage of the ester bond between PLGA and b-Glucan by hydrolysis [40] which leads to disassembly of the GNPs and further causing AMX come out from the assembly. These finding confirms our notion related to excellent gastric stability of AMX-GNPs and their site-specific drug release in presence of the overexpressed enzyme at inflammatory site.

3.4. *In vitro safety study*

Before going to assess *in-vitro* activity of nanoparticles, initially, we determined the safe concentration of AMX, βGlu, Blank NPs, AMX-GNPs and AMX-NPs on normal cell lines, including L929 and RAW264.7 cells. Cell viability was calculated using the MTT assay after drug treatment. As depicted in Fig. 2A-B, AMX concentration ranging from 20 to 50 μg/mL did not show any cytotoxicity to the L929 and RAW264.7 cells. However, concentration dependent reduction in cell viability was observed above 50 μg/mL (Fig. 2A-B). Therefore, the remaining cell-based study was carried out with AMX at safe concentration of 50 μg/mL. Further to ensure that AMX loaded GNPs and NPs did not adversely affect macrophage viability, an MTT assay was performed with AMX-GNPs/NPs. Where AMX-GNPs and AMX-NPs both did not show any cytotoxic effect (Fig. 2C). Additionally, the cytocompatibility of AMX-GNPs was performed on Caco-2 cell line, as AMX-GNPs primarily absorbed mainly through the intestinal epithelium after oral administration. Our results of the MTT assay (**Supplementary file,** Fig. S1F) confirmed that AMX-GNPs treatment was not exhibiting any potential cytotoxicity against Caco-2 cells. Further these studies results were validated with fluorescence based LIVE/DEAD assay on RAW264.7 cells. The AMX concentration of 50 μg/mL in GNPs and NPs was selected along with free β-Glu and blank NPS/GNPs. As illustrated in Fig. 2D, none of treatment exhibited cytotoxic effect compared to positive control, confirming that this concentration is safe concentration for further studies.

3.5. *Investigation of cellular uptake of nanoparticles*

Macrophages (Mϕ) play an important role in modulation of pancreatic inflammation, and it was observed that activated Mϕ are continuously recruited at the inflamed site[41]. Further we assumed that nanoparticles might get internalized into Mϕ and can contribute to achieve therapeutic potential in pancreatitis treatment by recruiting at the inflamed pancreas. Therefore, we assessed the cellular uptake of FITC tagged NPs (NPs) and FITC tagged GNPs (GNPs) specific to RAW264.7 cells. We performed the nanoparticle internalization on fibroblast cells (L929) as well, as illustrated in Fig. 2E, the differences in cell surface receptor present on Mϕ and fibroblast cells might contribute to the active targeting towards the Mϕ. We observed that fluorescence images (Fig. 2F) reflect minimal uptake of nanoparticles by fibroblast cells, which is attributed due to absence of Dectin-1 receptor on their surface [15]. At inflammatory stage, monocytes are polarized into M1 Mϕ, which are proinflammatory cells that furthers secret inflammatory cytokines. Therefore, to determine cell specific uptake, we incubated GNPs with polarized Mϕ. LPS was used to mimic M1 polarized Mϕ (inflammatory Mϕ). Confocal microscopy results (Fig. 2G) demonstrated that GNPs particles were significantly internalized (green fluorescence signals) by LPS induced Mϕ compared to plain nanoparticles. In contrast, the normal Mϕ (LPS untreated or negative control) exhibited minimal uptake of both NPs and GNPs. These findings were further corroborated by SEM (Fig. 2G and Fig. S2, **Supporting information**) and flow cytometric analysis (Fig. 2H). Overall, the above results confirm the efficient uptake of GNPs by M1 polarized Mϕ which is mediated by Dectin-1 receptors expressed on inflammatory Mϕ. The specific binding of β-Glucan to Dectin-1 receptor[42] facilitates the internalization of GNPs by M1 Mϕ.

3.6. *Assessment of inflammatory mediators*

The pathogenesis of pancreatitis is directly associated with excessive generation of nitric oxide (NO) and release of inflammatory cytokines. Furthermore, recent *in vitro* studies have reported AMX exhibits anti-inflammatory potential by suppressing inflammatory cytokines[17]. Therefore, we determined anti-inflammatory mechanism of AMX-GNPs against the LPS induced RAW264.7 cells. In control or untreated group, LPS activated macrophage (Mϕ) exhibits significant increase in level of inflammatory cytokines and nitrite level (Fig. 2I-L). In contrast, treatment with AMX-GNPs significantly reduced the levels of nitrite (NO_2^-) and cytokines such as IL-6, TNF-α and IL-1β in LPS activated Mϕ (Fig. 2I-L).

Notably, encapsulating AMX in GNPs enhanced the anti-inflammatory potential by reducing inflammatory markers and cytokines, possible through inhibition of Mϕ polarization to M1 subtype. Collectively, results proved that AMX-GNPs are cytocompatible and effectively target the inflammatory Mϕ and reduce the potential markers of inflammation.

3.7. *Macrophage polarization study*

Macrophages (Mϕ) are one of the key immune cells of body, that plays a crucial role in maintaining both physiological and pathological functions. In normal physiological condition, these cells are present in the form of monocytes. They can be polarized into two different phenotypic types: M1 (pro-inflammatory Mϕ) and M2 macrophage (anti-inflammatory Mϕ), depending on the type of stimuli. M1 polarized Mϕ are generally involved in acute and chronic inflammation, tissue fibrosis and pathogen infection. While M2 polarized Mϕ plays key role in anti-inflammatory response, tissue regeneration and remodeling phenomena [43].

To emphasize the active role of polarized Mϕ in pancreatitis [44], we further investigated the effect of different treatments on Mϕ reprogramming (Fig. 3A). These two types of Mϕ can be distinguished by their surface markers: M1 polarized Mϕ have CD80 and CD86, M2 polarized Mϕ exhibit CD163 and CD206.

To monitor the effect of AMX, βGlu and AMX-GNPs treatment on Mϕ reprogramming we first performed Immunocytofluorescence (ICF) staining on RAW cells, the ICF images (Fig. 3B) with polarized Mϕ, stained with CD80 antibody (red) represents M1 polarized Mϕ, and the cells stained with CD163 antibody (green) represents the M2 polarized Mϕ. Further, the observation in AMX and βGlu treated groups showed little increment in ratio of M2/M1 positive cells, which shows less anti-inflammatory activity. Subsequently, we found that AMX-GNPs treatment group showed significant increment in ratio of M2/M1 positive cells (Fig. 3B-C) compared to M1 control group (only LPS treated). While AMX-GNPs treatment with M2 Mϕ (IL-4 induced RAW264.7 cells)

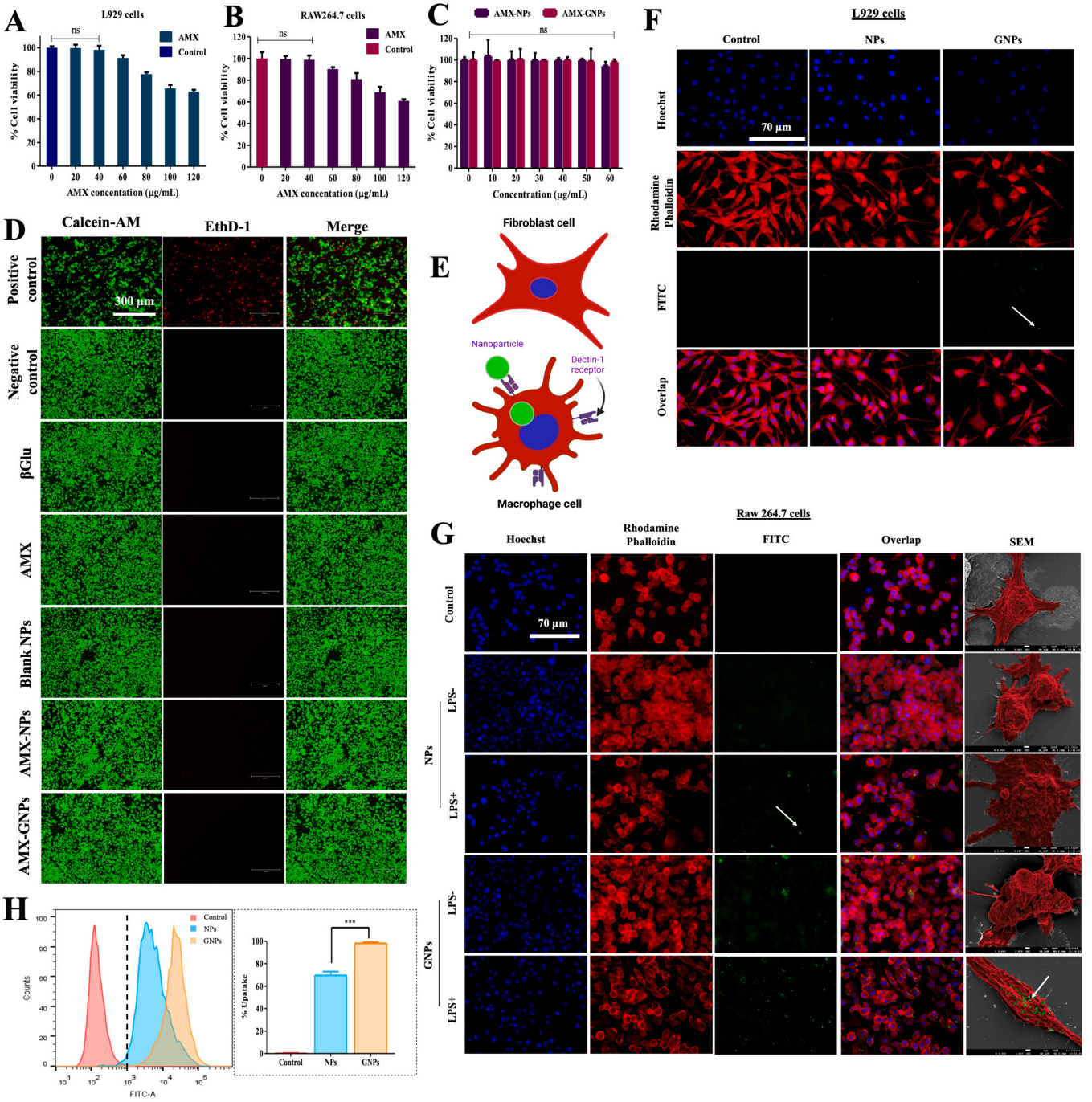

(caption on next page)

Fig. 2. *In-vitro* assessment of cytocompatibility of AMX-GNPs (A). MTT assay on L929 cells after treatment with AMX (B). MTT assay on RAW264.7 cells after treatment with AMX (C). Cell viability assessment of AMX-loaded GNPs (AMX-GNPs) and AMX-loaded NPs (AMX-NPs) against RAW264.7 cells (D). Live and dead cells staining after treatment RAW264.7 cells with β-Glucan (βGlu) at concentration of 50 μg/mL, AMX at concentration of 50 μg/ mL, Blank NPs at concentration of 1 mg/ mL, NPs with equivalent dose of 50 μg/ mL AMX and GNPs with equivalent dose of 50 μg/ mL to AMX. Green fluorescence represents Calcein-AM staining (Live cells) and red fluorescence represent EthD-1 staining (Dead cells). Images were captured with scale bar = 300 μm. Cellular uptake study for the GNPs (E). Diagrammatic representation illustrating the differences between macrophage, fibroblast cell surface and receptor-mediated uptake of GNPs. (F) Cellular uptake of FITC-tagged GNPs (GNPs) and FITC-tagged GNPs (NPs) in L929 cells, nanoparticles exhibit green fluorescence and rhodamine-phalloidin (red cytoskeleton), Hoechst 33,342 stained nucleus (blue fluorescence), Images were captured with scale bar = 70 μm. (G). Comparative images for cellular uptake of GNPs and NPs in the presence and absence of LPS, in RAW264.7 macrophages analyzed by CLSM and SEM analysis (H). Flow cytometric analysis for GNPs and NPs uptake in LPS activated macrophages, where control or untreated group is denoted in red color, NPs and GNPs group is represented in blue and orange color, respectively. Level of significance = $p < 0.001$*** GNPs vs NPs. *In-vitro* anti-inflammatory activity of β-Glucan (βGlu), AMX and AMX-GNPs (AMX-loaded nanoparticles GNPs) (I) Assessment of Nitrite levels (J) IL-6 level (K). TNF-α (L) IL-1β in LPS induced RAW264.7 cells (LPS +). All values are presented as means ± SEM (n = 3). Level of significance $p < 0.001$*** LPS + vs LPS- group, $p > 0.05$ ns, $p < 0.05$* & $p < 0.01$** LPS + AMX vs LPS + group, $p < 0.05$*, $p < 0.01$**& $p < 0.001$*** LPS + AMX-GNPs vs LPS + group. (For interpretation of the references to color in this figure legend, the reader is referred to the web version of this article.)

showed no effect which infers that AMX-GNPs treatment only arrest M1 polarization keeping M2 Mϕ unaffected.

Furthermore, to ascertain this notion, we performed quantitative estimation by flow cytometric analysis (Fig. S3A and S4A, **supporting information**). M1 polarized (LPS activated RAW264.7 cells) and M2 polarized (IL-4 activated RAW264.7 cells) Mϕ were incubated with different treatment such as AMX, βGlu and AMX-GNPs (Fig. 3D-H). The flow cytometric analysis (Shown in **Supplementary File**, Fig. S3&4) was carried out to check the expression of M1 (CD80 and CD86) and M2 (CD163 and CD206) Mϕ surface marker. Additionally, F4/80 and CD11b were used as pan-Mϕ markers to define Mϕ cells. The results showed that percentage of $F4/80^{+}CD206^{+}$ Mϕ and $F4/80^{+}$ $CD163^{+}$ Mϕ was significantly increased in M1 polarized Mϕ (Fig. 3D&F and Fig. S3, **supporting information**) after AMX-GNPs treatment as compared to untreated M1 polarized Mϕ cells (LPS + group). In contrast, % of $F4/80^{+}$ $CD80^{+}$ Mϕ and $F4/80^{+}$ $CD86^{+}$ Mϕ was significantly reduced (Fig. 3E&G) in M1 polarized Mϕ after AMX-GNPs treatment compared to untreated M1 polarized cells (LPS + group). Post treatment with AMX and βGlu, the percentage of CD80 and CD86 positive cells was equally reduced upto 25 % and 17 % respectively in both treatments compared to LPS^{+} group. However, AMX-GNPs treatment caused 65 % and 90 % reduction in CD80 and CD86 positive cells (Fig. 8G&E) than LPS + group. Further, LPS activated cells after AMX-GNPs incubation showed higher expression of CD206 and CD163 (Fig. 8D&E) upto 40 % and 6.68 % respectively as compared to LPS + group. We also checked whether AMX, βGlu and AMX-GNPs treatment can modulate M2 polarized (IL-4 + cells) Mϕ (Fig. S4A, **Supporting information**). As results depicted in **supplementary file**, Fig. S4B&C showed effect of treatment on CD80, CD86 and CD206, CD163 positive Mϕ population. In (Fig. S4B-D, **Supporting information**) clearly reflected the AMX, βGlu and AMX-GNPs group did not show any effect on M2 polarized Mϕ cells.

All these results suggested that AMX-loaded GNPs formulation is more specifically target the M1 Mϕ and it has ability to repolarize M1 into M2 type Mϕ which helps to reverse the inflammation in pancreatitis.

3.8. M cell targeting ability of GNPs

For active targeting to pancreas after oral administration of GNPs, specifically M cells are involved in transportation of nanoparticles through the intestinal PPs [45]. We tested this notion using *in vitro* M cell model. As shown in Fig. 4A, the model was established by Caco-2 and Raji B cells co-culture method, where Raji B cells is mimicking intestinal M cells. After M cell model was established, and we treated the monolayer with FITCtagged GNPs/NPs formulation and at the end of the study we measured the TEER (Transepithelial Electrical Resistance) value of every group, and we found that GNPs and NPs treatment did not show any changes in TEER value (Fig. 4B), which indicated that both of the formulations did not interfere with epithelial tight junctions. Further to ascertain if the uptake was mediated by M cells, here we used M cells blocker laminarin (In; inhibitor) which can block Raji B cells Dectin-1 receptor specifically[46]. So, we carried out the study in presence and absence of inhibitor and measured particle concentration based on fluorescence intensity. We observed that GNPs concentration was significantly higher in basolateral compartment compared to NPs treated group. As depicted in Fig. 4C, NPs was detected at high amount in apical compartment of trans well plate. Subsequently, the monolayer cells were pre-incubated with inhibitor (laminarin), showed GNPs nanoparticles were stayed into apical compartment with higher amount (Fig. 4C), which indicate that GNPs potentially cross intestinal junction via Dectin-1 receptor-mediated internalization by M cells. Further the presence of β-Glucan on surface of nanoparticles confirms the notion, that GNPs can be internalized by intestinal M cells, after oral administration.

3.9. In vivo safety study

To evaluate the *in-vivo* safety profile of the AMX-loaded GNPs nanoparticle (AMX-GNPs), an acute oral toxicity study was conducted on Wistar rats. In course of 14-day *in-vivo* toxicity assessment, the rats were administered with daily dose of AMX-GNPs orally, while the untreated rats served as the control group (Fig. 5A). We observed the animals for changes in the body weight, which is essential parameter to know the health status. Data suggest that there was a no significant difference in body weight observed in the AMX-GNPs treated group as compared to the untreated group, as explained in Fig. 5B (ns, $P > 0.05$). Furthermore, we performed organ toxicity assessment based on biomarkers for the liver and kidney.

The blood and urine samples were collected at the end of the study and the biochemical parameters were assessed, such as alanine transferase (ALT), serum glutamic oxaloacetic transaminase (SGOT), serum glutamic pyruvic transaminase (SGPT) aspartate aminotransferase (AST) and creatinine level to assess the vital organ functions after treatment. The results of the biochemical assessment (including liver and kidney function tests) indicated no significant alteration (ns, $P > 0.05$) after 14-days of oral dosing as compared to the untreated group (Fig. 5C). Further, we performed the study to assess histological changes in the vital organs, such as liver, kidney, brain, and spleen. Hematoxylin and eosin (H&E) staining was performed on vital organ, and the results (Fig. 5D) indicates that no evidence of toxicity or histological alteration in vital organ.

Overall, no significant changes were observed in the histological and biochemical parameters or body weight after AMX-GNPs treatment, suggesting AMX loaded GNPs formulation is non-toxic and safe for biological systems.

3.10. Biodistribution of GNPs

For safe and effective delivery of the drug, biodistribution of the nanoparticle is crucial parameter after oral administration. In our study the nano-formulation should effectively bypass the acidic environment of stomach and deliver the drug at target site without affecting other

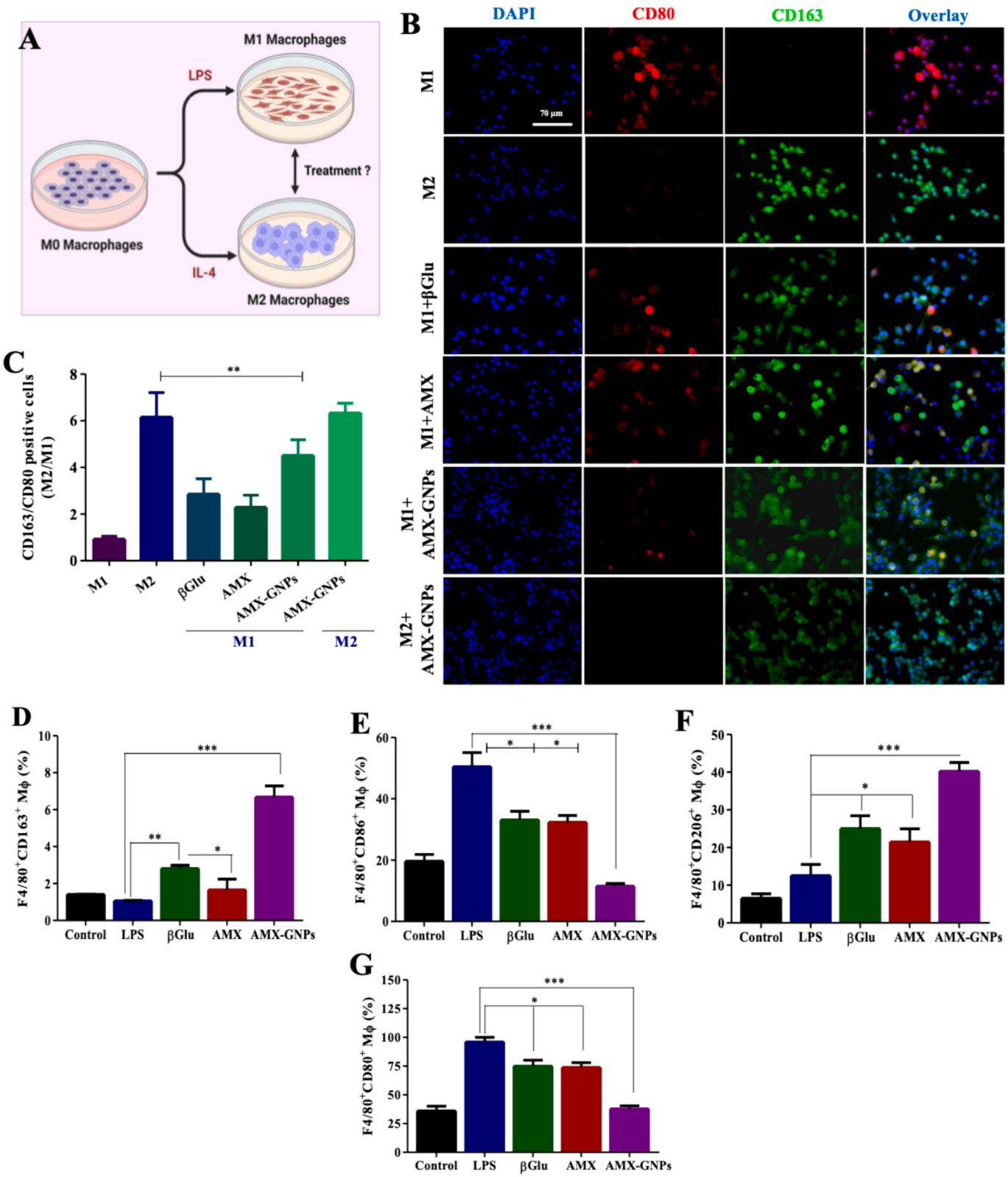

Fig. 3. Macrophage polarization assessment (A) Schematic of macrophage phenotypes after activation with LPS and IL-4, experiments were depicted as βGlu, AMX and AMX-GNPs causing M1 macrophage or M2 macrophage polarization. (B) Differentiation of macrophage phenotype analysed with immunofluorescence staining of CD80 and CD163 after treatment (C) The ratio of CD163 and CD80 positive cells in M2 &M1 macrophage after drug treatments. Graphs are presented as mean ± SEM (n = 3). Level of significance $p < 0.001$** M1 + AMX-GNPs compared M2 control group. Flow cytometric analysis for identification of CD206, CD163 positive cells and CD80, CD 86 positive cells population (D). Graphical representation of percentage positive CD163 cells (E). Percentage positive CD86 cells (F). Percentage positive CD206 cells (G). Percentage positive CD80 cells. All values are presented as means ± SEM (n = 3). Level of significance $p < 0.001$*** & $p < 0.01$** GNPs treated M1 polarized macrophage vs LPS + group, $p < 0.05$*& $p < 0.01$** β-Glucan treated M1 polarized macrophage vs LPS + group, $p < 0.05$* AMX treated M1 polarized macrophage vs LPS + group.

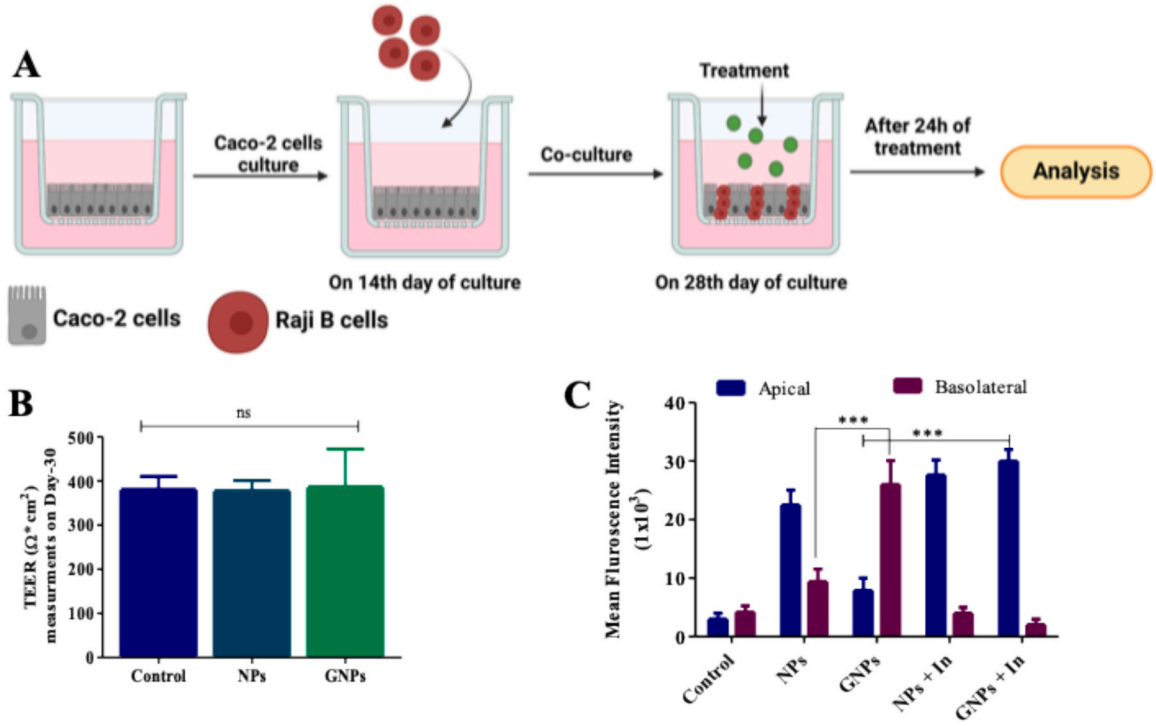

Fig. 4. Assessment of M cell targeting ability of GNPs. (A) Schematic illustration of established M cell model using Caco-2 and Raji B cells co-culture (B) TEER (Transepithelial Electrical Resistance) value of monolayer after incubation with FITC tagged GNPs (GNPs) and FITC tagged NPs (NPs). (C) Transportation of nanoparticles from the monolayer with and without inhibitor. All values are presented as mean ± SEM (n = 3). Level of significance for TEER measurement $p > 0.05$ (ns = non-significant) GNPs vs NPs group. $p < 0.001$*** GNPs concentration in basolateral compartment vs NPs group, $p < 0.001$*** GNPs concentration in apical compartment with presence of laminarin (In; inhibitor) vs NPs group.

organs. We performed biodistribution using ICG (Indocyanine green) as a fluorescent tracking dye and the encapsulation of ICG in GNPs/NPs (GNPs, NPs) was confirmed by IVIS imaging system (Fig. S5A, **Supplementary File**). After oral treatment with NPs and GNPs, were examined for the biodistribution with IVIS analysis (*in vivo* imaging system). In this, diseased animals were received with oral dose of ICG loaded NPs, GNPs and at predetermined time points and the animals were sacrificed. Three rats from each group were euthanized after 1 h of post oral treatment and whole gastrointestinal tract was isolated and IVIS analysis was carried out. The increased fluorescence in Fig. 6A represents the disassembly of NPs specifically in GI tract of animals after 1 h. As per our hypothesis the NPs undergo hydrolysis or disassembles in acidic pH [47] or stomach pH as shown from our release study in Fig. 1J. Here in the biodistribution we similarly observed that the NPs are showing maximum fluorescence in GIT. The NPs containing ICG dye resulting disassembly and release of the dye in stomach showed the strong fluorescence within 1 h (Fig. 6A). Consequently, GNPs treated animals exhibited less fluorescence signal only in a smaller area of stomach. Whereas β-Glucan surface conjugation with PLGA, forming pH-resistant layer outside the PLGA core that protect GNPs from harsh acidic environment of stomach after oral administration.[48].

Subsequently, 5 h of post oral treatment, GIT with all vital organs and pancreas were excised. The *ex-vivo* IVIS images (Fig. 6A-B) displayed that NPs treated group showed strong fluorescence signal in all over stomach and small intestine, this shows that NPs were degraded by acidic condition of stomach, representing pre-systemic absorption and non-specific distribution. However, animals treated with GNPs shows no signal in stomach and emitted uniform fluorescence signal in small intestine, more specifically at the area of PPs. In the same group, we also acquired *ex vivo* IVIS images of heart, kidney, lungs, brain, spleen, liver and pancreas (Fig. 6B). They showed no fluorescence signals in any vital organs of both groups, because of 5 h post oral treatment schedule is not enough to reach the systemic circulation. In contrast only pancreas showed detectable fluorescence signal in GNPs and NPs treatment group. Which confirms our notion of the targeted drug release in pancreatic environment.

The difference in fluorescence intensity was assessed by plotting the graph between Average Radiant Efficiency (p/s/cm^2/sr)/(μW/cm^2) and different organs. The graph (Fig. 6D) shows that the fluorescence signal was significantly higher in the pancreas of the GNPs-treated group as compared to the NPs-treated group. We also conducted *ex-vivo* IVIS imaging of PPs and MLN (Fig. 6C), which showed significantly higher fluorescence signals in PPs and MLN in the GNPs group as compared to NPs group (Fig. 6E). Additionally, we also assessed the biological distribution of GNPs and NPs post-absorption. Fig. S5B shows in **Supplementary File**, after 24 h of oral treatment, nanoparticles showed higher fluorescence signals in the liver, lungs, heart, and kidneys in the NPs treated group as compared to the GNPs group. In comparison we observed strong signal in the spleen and pancreas of GNPs group animals.

The results indicate that, orally administered NPs were unable to bypass pre-systemic metabolism and were primarily transported to the liver and heart, with excretion mainly occurring through the kidneys. However, the GNPs was mostly distributed in pancreas and spleen after oral administration.

3.11. Route of drug absorption

Every nano-formulation that administered orally follows intestinal absorption, either by entering the intestinal lymphatic pathway or directly into systemic circulation[49]. In biodistribution study, we demonstrated that GNPs nanoparticles were absorbed through intestine and actively reached the target site. To determine the route of GNPs delivery, we utilized *in-situ* loop formation method (ref), in which we made intestinal loop by simple ligation technique with intestine and incubated the ICG-tagged GNPs (GNPs) formulation. After incubation,

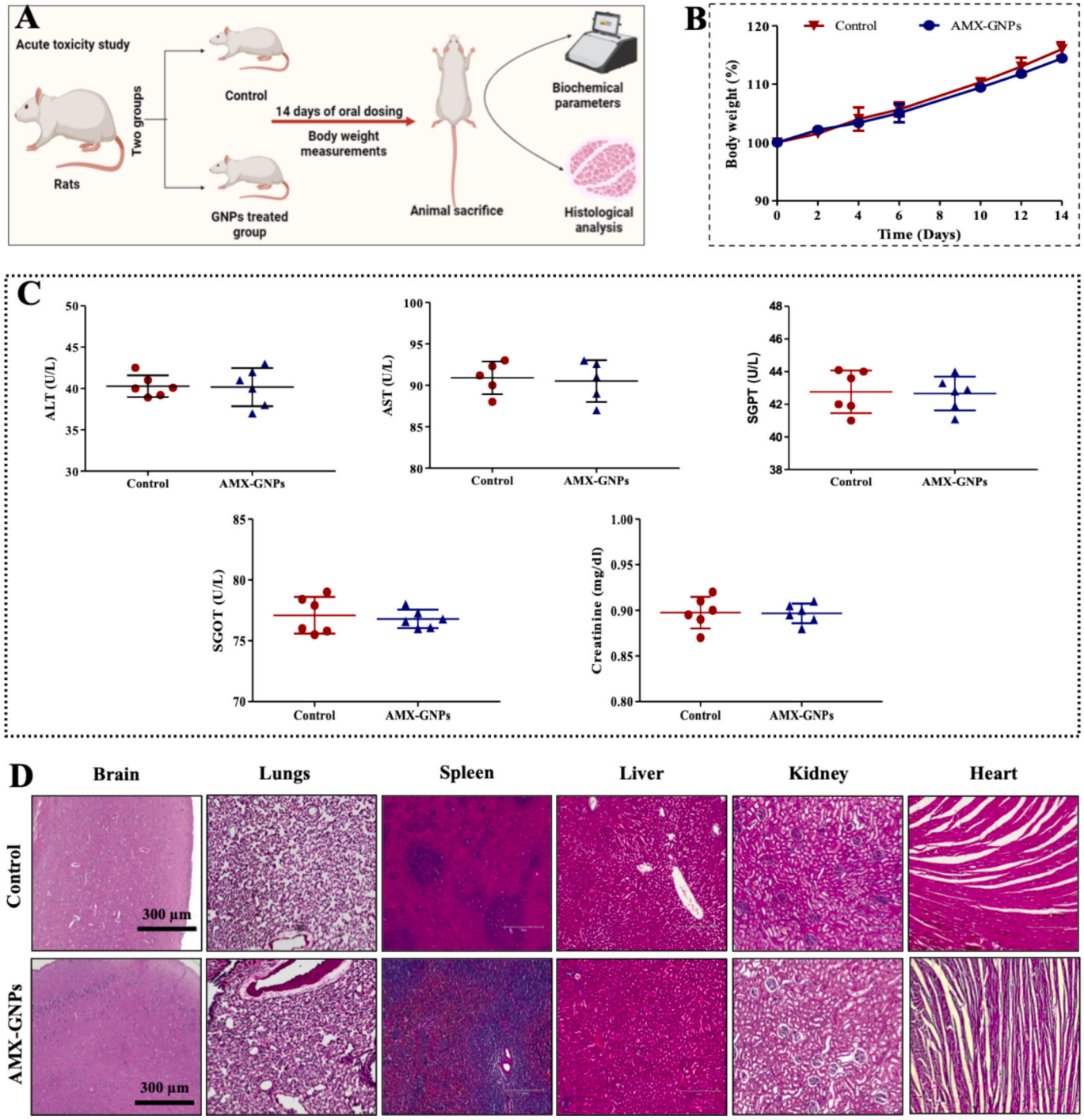

Fig. 5. *In-vivo* safety profile of AMX-GNPs in Wistar rats. (A). Illustration of acute oral toxicity study and treatment schedule. (B) Percentage of body weight of animals (C) Analysis of biochemical parameter (alanine transferase (ALT), serum glutamic oxaloacetic transaminase (SGOT), serum glutamic pyruvic transaminase (SGPT) aspartate aminotransferase (AST) and creatinine level) after AMX-GNPs treatment. All values are presented as mean ± SEM (n = 3) (D). Histological analysis using H&E staining of Brain, Lungs, Kidney, Spleen, Liver and Heart.

intestinal loop was carefully retrieved, intestinal villi, PPs and MLS was separated. These tissue samples were analysed using confocal microscope and IVIS system.

A schematic representation of M cell distribution is depicted in Fig. 6F. Immunofluorescence and CLSM images of tissue sections indicate that ICG-tagged GNPs (green fluorescence) were effectively co-localized inside the M cells (red fluorescence) of PPs and epithelial villi (Fig. 6F). Further, *ex-vivo* fluorescence image of MLS showed fluorescence intensity within lymphatic capillaries due to nanoparticle absorption (Fig. 6G). These results revealed that mesenteric lymphatic pathway was involved in intestinal absorption of GNPs nanoparticles after oral administration.

To confirm that GNPs specifically follows M cell-based ILS pathway, a same study was conducted using cycloheximide which inhibit M cells mediated ILS transport. In this, animals were pretreated with cycloheximide before the development of the intestine *in situ* Loop. After incubating with GNPs, the animals were euthanized, and tissues were examined. The results (Fig. 6H) showed no green fluorescence particles

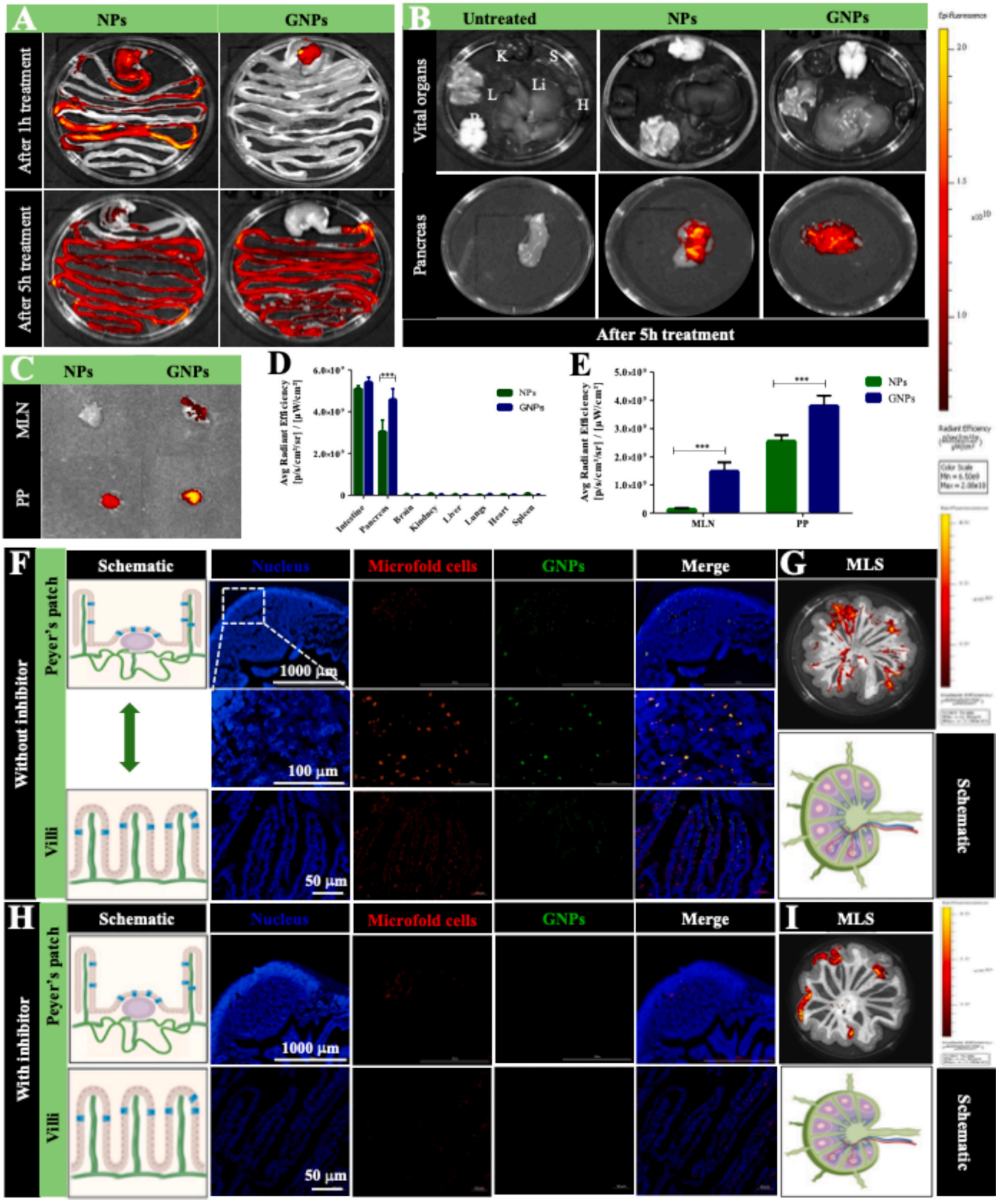

(caption on next page)

Fig. 6. Targetability of ICG-tagged GNPs and NPs after oral administration (A) Fluorescent IVIS images of GI tract of animal depicting the drug distribution after 1 h and 5 h of oral treatment of NPs, GNPs. (B) Ex-vivo fluorescence images of vital organs (H; Heart, K; Kidney, B; Brain, L; Lungs, Li; Liver, S; Spleen) along with pancreas, after 5 h of oral treatment (C) Typical ex-vivo IVIS images of Peyer's patch (PP) and Mesenteric Lymph Node (MLN) followed by oral treatment with nanoformulation (D&E). Graphical illustration of distributed fluorescence signal of isolated organs and Peyer's patch (PP), Mesenteric Lymph Node (MLN) and the difference in fluorescence intensity was assessed by plotting a graph between Average Radiant Efficiency ($p/s/cm^2/sr)/(\mu W/cm^2$) and tissues. All values are represented as means ± SEM (n = 3). The level of significance of fluorescence intensity in Pancreas, MLN, PP; $p < 0.001$*** in GNPs vs NPs group. Determination route of drug absorption of GNPs nanoformulation using *in situ* loop method. (F) Pictures represents the M cell distribution in PPs (Peyer's patches), intestinal villi and CLSM immunofluorescence images of PPs, Villi section. The green fluorescence signal represents ICG-tagged GNPs (GNPs) and M cells which are visualized by the red fluorescence. (G). Schematic representation of MLS (Mesenteric Lymphatic System) and IVIS images indicates GNPs absorption of GNPs in MLS. (H) The schematic gives an idea about the PPs (Peyer's patches) and intestinal villi,CLSM images of cycloheximide (inhibitor) pretreated animal (I) cycloheximide is preventing the intestinal absorption of GNPs in M cells and MLS (IVIS analysis). n = 3. (For interpretation of the references to color in this figure legend, the reader is referred to the web version of this article.)

were present inside PPs and epithelial villi, due to cycloheximide mediated inhibition of ILS transportation, which was preventing the nanoparticles co-localization within lymphatic tissue or M cells (Fig. 6H-I). These findings suggest that the absorption of GNPs after oral administration primarily occurs through the ILS pathway.

The collective results of the biodistribution study and the investigation into the route of drug absorption indicate that after oral administration, particles follow the intestinal lymphatic route, which was further responsible for GNPs accumulation in the pancreas.

3.12. Therapeutic efficacy against acute pancreatitis

Based on the *in vitro* anti-inflammatory activity and *in vivo* targeting ability of GNPs, we investigated the therapeutic efficacy of AMX-GNPs against L-arginine induced Acute Pancreatitis (AP) model. Experimentally, AP model was established by injecting a high dose of L-arginine and confirmed by measuring standard clinical marker such as serum lipase and amylase level. The rats were distributed as AMX, βGlu and AMX-GNPs groups for respective treatment with proper controls. A schematic representation of model development and treatment schedule is depicted in Fig. 7A.

As data represented in Fig. 7B-E, the AP model was characterized by typical symptoms like pancreatic edema, higher pancreas to body weight ratio, and elevated levels of serum amylase upto 550 ± 49.0 U/L and serum lipase value upto 103 ± 12.8 U/L relative to healthy group (Fig. 7B-E). We observed that there was no significant difference in pancreatic edema, pancreas to body weight ratio and serum amylase in β-Glucan (βGlu) treated AP animals compared to disease animal (AP group), except the serum lipase level was found to be notably decreased. Free AMX was also found to be showing activity against AP, which significantly reducing the pancreas to body weight ratio ($p < 0.05$*), and simultaneously the serum amylase and serum lipase level ($p < 0.01$**) compared to AP model group,which was also found to be reduced. However, AMX-GNPs treatment showed highly significant effect ($p < 0.001$**) against AP disease by lowering the pancreatic edema, pancreas to body weight ratio, serum amylase and serum lipase level. Moreover, in comparison to AMX this effect was also significant (Fig. 7B-E). These observations suggest that AMX-GNPs showed potential effect in AP by reducing its key symptoms.

In the next step, we assessed the therapeutic effect of AMX-GNPs at the histological level, specifically in pancreatic and lung tissues, as AP is often associated with lung injury. The histological data indicates that the lungs and pancreas of the healthy group exhibited characteristic histopathology in H&E staining. Healthy pancreas showed normal interlobular and intralobular spaces, typical acinar cell structure, or pancreatic islets, normal parenchymal cells and no infiltration of immune cells, also there was absence of signs of edema or infiltration of inflammatory cells with a normal alveolar structure in lung tissue (Fig. 7G). In the AP model group, L-arginine caused major histopathological alterations in pancreatic and lung tissue as seen in H&E staining (Fig. 7F). AMX and βGlu treatment in AP animals resulted a slight reduction in pathological score compared to the AP model group, although the difference was not statistically significant. When disease animal treated with AMX-GNPs we observed significant improvement in histological outcomes. It caused marked reduction in histopathological score of the pancreas.This was accompanied by recovery in acinar and pancreatic cell morphology, the absence of hemorrhage and fat necrosis, along with an improvement in lung histology was observed similar to healthy group histoarchitecture (Fig. 7F-G). The H&E staining results showed that AMX-GNPs treatment improved the histological alterations against AP pathological injury of the pancreas and lungs.

Additionally, histopathological changes of pancreatic tissues after treatment were also confirmed by Masson's trichrome staining (Fig. 7H). The % fibrotic area was calculated based on positive staining in periductal tissue, acinar cells and interlobular space [50]. In AP model group, pancreatic tissue exhibited 40 % fibrotic area that indicated pancreatic fibrosis with intralobular sclerosis. In contrast, AMX-GNPs treatment showed only 8.5 % pancreatic fibrosis, which significantly ($p < 0.001$***) reduced as compared to disease group (Fig. S6A, **supporting information**), which depicts that AMX-GNPs has strong potential to reduce the pancreatic fibrosis in AP rat.

AMX is a selective inhibitor of TBK1/IKKε, that regulates the downstream signaling pathways by inhibiting NF-κB activation in various diseases [51]. To further understand the mechanism of AMX-GNPs after treatment in AP disease, we performed immunohistochemical (IHC) staining for NF-kB, IL-6 and IL-4 markers. We noticed a potential increment in immunopositive cells of NF-kB and IL-6 in AP rats (Fig. 7H and Fig. S6B-C, **Supporting information**) due to development of inflammation in the pancreas. Subsequently, we also compared the AMX treatment group to AP model group and found significant reduction ($p < 0.05$*) in the % of IL-6 and NF-kB positive cells (Fig. 7H and Fig. S6B-C, **supporting information**). However, AMX-GNPs treatment effect was highly significant ($p < 0.001$***) in terms of reduction in percentage of IL-6 and NF-kB positive cells when compared to the AP group. Additionally, the AMX-GNPs treatment also showed significant effect as compared to free AMX treated group (Fig. 7H and Fig. S6B-C, **supporting information**).

Furthermore, we evaluated IHC staining of anti-inflammatory marker, which showed βGlu itself significantly increase the % IL-4 immunopositive cells (Fig. 7H and Fig. S6D, **supporting information**), likely due to immunomodulatory effect (macrophage polarization) of βGlu. Notably, the AMX-GNPs treatment showed potential increase ($p < 0.001$***) in the IL-4 expression in AP rats.

All IHC results indicated that AMX-GNPs treatment against AP disease showed potential effect on NF-kB, IL-6 and IL-4 immunopositive cells. The reduction might be attributed due to the additive effects of AMX and β-Glucan which overall significantly inhibits the NF-κB, IL-6 and activate IL-4 expression (Fig. 7H).

NOS2 is prominently expressed in pro-inflammatory or M1 Mϕ and plays a significant role in exacerbating inflammatory condition through NO generation. NOS2 is well reported marker that is expressed in M1 polarized Mϕ [52,53]. So, to assess the *in-vivo* effect of AMX-GNPs on Mϕ polarization in diseased animals, we performed the immunofluorescence (ICF) staining to evaluate NOS2 expression in the pancreatic tissue. The immunostaining results demonstrated a significant reduction in NOS2 (iNOS) expression in AMX-GNP treated group (Fig. S8, shows in

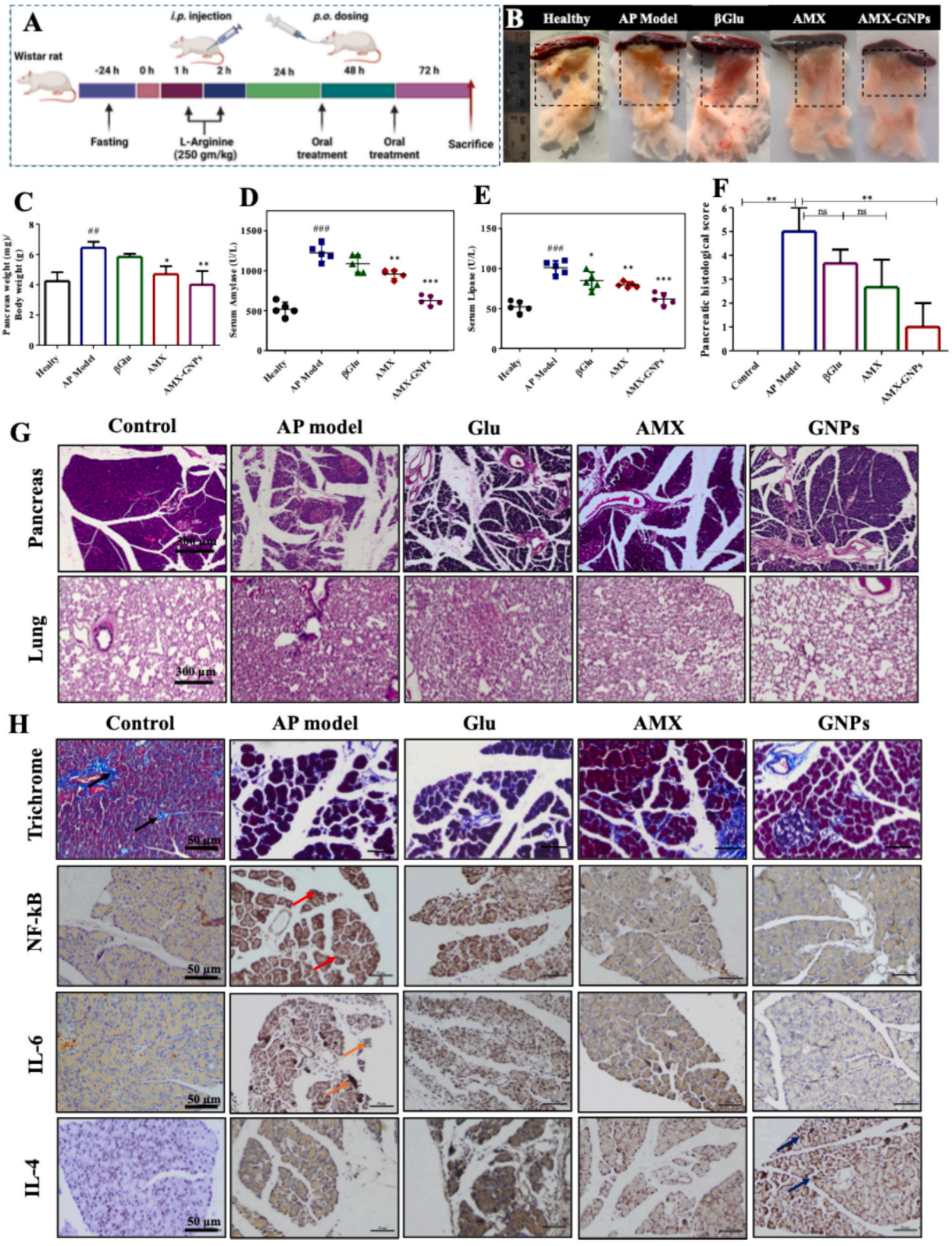

Fig. 7. Therapeutical efficacy of AMX-GNPs against AP model. (A). Schematic representation of experimental model and treatment timeline. (B). At the end of treatment schedule, pancreas was isolated, and images were captured for morphological assessment. (C) Graphs represent the pancreas to body weight ratio of every group. (D&E) Serum amylase and lipase level of treatment group, disease (AP) and healthy group (control) (F) Histopathological scoring of pancreatic tissue, scoring was done on the basis of representative H&E staining. (G). Histopathological alterations in pancreas and lung were analysed by H&E staining (scale bar = 300 μm) (H). Anti-inflammatory effect of βGlu, AMX, AMX-GNPs was evaluated using Masson's trichrome and IHC staining for NF-kβ, IL-6 and IL-4 expression in pancreatic tissue (scale bar = 50 μm). All graphs are presented as mean ± SEM (n = 3). Level of significance $p < 0.001$***, $p < 0.01$**, $p < 0.05$* & ns = $p > 0.05$.

Supplementary File). This result was corroborated with *in-vitro* studies we performed earlier which showed the treatment effect on Mϕ reprogramming and indicated that AMX-GNPs has potential to attenuate or modulate M1 Mϕ polarization in disease condition.

Subsequently, we performed a gene expression study on pancreatic tissue to evaluate the immunomodulatory effect of AMX-GNPs (Fig. S9, shows in **Supplementary File**). We evaluated the gene expression by RT-PCR analysis and quantified the mRNA levels of pro-inflammatory cytokine genes (IL-1β, TNF-α, and IL-6), as well as M2 and M1 polarized Mϕ cell surface marker CD206 and NOS2, following oral treatment in diseased animals.

The L-arginine induced, acute pancreatic injury caused marked elevation ($p < 0.001$***) in mRNA levels of IL-6, TNF-α, IL-1β, NOS2 and reduced CD206 genes expression in Wistar rat (Fig. S9A-E, **Supporting information**). While gene expression of M1 Mϕ associated gene (NOS2) include pro-inflammatory cytokine gene (specifically TNF-α, IL-1β and IL-6) were observed to be reduced ($p < 0.05$*) as compared to AMX treated group (Fig. S9A-C, **Supporting information**). However, βGlu treatment selectively upregulated the expression of M2 Mϕ associated gene CD206 (Fig. S9E, **Supporting information**). Notably, the treatment with AMX-GNPs was responsible for approximately two-fold reduction in IL-6, TNF-α, IL-1β, NOS2 gene expression and upregulated the M2 Mϕ associated gene CD206 (Fig. S9A-E, **Supporting information**). Here, we observed that potential effect of AMX encapsulated GNPs which is most likely attributed due to synergistic effect of AMX and βGlu within the nano formulation and that collectively suppress the expression of inflammatory cytokines and macrophage related gene.

In summary, our results demonstrated that orally administered AMX-GNPs shows significant therapeutic efficacy against AP, primarily due to the combined effect of AMX and β-Glucan. AMX is anti-inflammatory agent, while β-Glucan remains over the surface of the nanoparticles, which facilitates the targeted drug delivery and provides an additional immunomodulatory effect. The treatment with AMX-GNPs successfully attenuated pancreatic inflammation and fibrosis, as well as reduced levels of amylase and lipase enzymes in the bloodstream, providing a potential alternative for managing AP. The Mechanistic studies, using immunohistochemical, immunofluorescence and gene expression analyses provided inside into the molecular mechanism by which AMX-GNPs reduce the inflammation and contribute to its positive effects in treating AP.

3.13. Therapeutic efficacy against chronic pancreatitis

In previous *in-vivo* studies revealed that AMX-GNPs exhibit therapeutic potential after oral administration against acute pancreatitis (AP). These findings prompted us to investigate whether long-term treatment with AMX-GNPs could be helpful in treating the Chronic Pancreatitis (CP). We established experimental model of CP in Wistar rats by long term exposure with L-arginine and optimized protocol for CP model which is depicted in Fig. 8A. The disease progression and confirmation of models was confirmed by measuring a standard clinical marker such as serum lipase and amylase level. The rats were divided into a five groups CP model, healthy, AMX, βGlu and AMX-GNPs treatment group. The animals were received oral dose following the dosing schedule as mentioned in Fig. 8A.

CP is a chronic inflammatory disease characterized by the slow and irreversible destruction of pancreatic parenchymal cells, resulting in tissue atrophy or fibrosis [54]. We observed extensive atrophy in pancreatic mass (Fig. 8B) in CP-developed animals due to inflammation. Body weight and pancreas weight was measured, then pancreas to body weight ratio was calculated at the end of study to understand the health and progression of therapy. The pancreas to body weight ratio was significantly decreased in CP model (Fig. 8C), while serum amylase and lipase levels were observed to be elevated upto four times compared to healthy control (Fig. 8D-E). βGlu treated group, showed no visible difference in pancreas to body-weight ratio also the serum amylase and lipase levels in CP rats, however mild improvement might be observed in pancreatic morphology as compared of CP model group (Fig. 8C-E). Further, the long-term oral treatment of AMX exhibited potential therapeutic activity against CP, as evidenced by improvement in tissue morphology (Fig. 8B) and significant reduction in pancreas to body weight ratio ($p < 0.05$*), serum amylase and lipase levels ($p < 0.05$*) in CP rats.

Further, the long-term oral treatment with AMX-GNPs showed the highest efficacy ($p < 0.001$**) against CP disease by reformation in pancreatic tissue and improvement in pancreas to body weight ratio, additionally serum amylase and lipase levels also observed to be in the normal range.We also observed that biological effect of AMX-GNPs was significant as compared to AMX treated group (Fig. 8C-E). These results suggest that AMX-GNPs hold strong therapeutic potential for CP treatment and its better alternative to the existing therapies.

In the next step, we assessed AMX-GNPs in CP model at histological level in pancreatic and lung tissues. The histoarchitecture of lungs and pancreatic tissue of the healthy rats revealed characteristic histopathology in H&E staining. Healthy pancreas showed normal interlobular and intralobular spaces, typical acinar cell structure, or pancreatic islets, with normal parenchymal cells and no infiltration of immune cells, also there was no prominent edema or infiltration of inflammatory cells having normal alveolar structure in lung tissue (Fig. 8G). Further, the CP rats exposed with repeated dose of L-arginine, exhibited major histopathological alterations in pancreatic tissue and lung pathology in H&E staining, which are represented in Fig. 8F&G. Oral treatment with β-Glucan or AMX in CP rats showed a mild reduction in pathological score of pancreatic and lung tissues, although these improvements were not statistically significant as compared to the untreated CP model group. The AMX-GNPs treatment significantly improved ($p < 0.01$**) histoarchitecture as compared to CP group, by reducing the histopathological score of the pancreas, which results in recovery of acinar and pancreatic cell morphology, and the absence of hemorrhage and fat necrosis, along with a recovery in lung histology observed looks similar to healthy group (Fig. 8F&G). All results of H&E staining suggested that prolonged treatment with AMX-GNPs could reduce CP associated histopathological injury of pancreatic and lungs tissue.

Subsequently, histopathological changes of pancreatic tissue after treatment were also confirmed by Masson's trichrome staining (Fig. 8H). The percentage fibrotic area was calculated on the basis of positive staining in periductal tissue, acinar cells and interlobular space [50]. We observed that 80–90 % fibrosis in pancreatic tissue of disease rat which represented fibrosis with extensive intralobular sclerosis are developed. In contrast, AMX-GNPs treatment showed (Fig. S7A **Supplementary File**) marked reduction in pancreatic fibrosis upto 35 %. This effect was highly significant ($p < 0.001$***) as compared to disease group, which demonstrated the AMX-GNPs shows significant potential to reduce the pancreatic fibrosis in CP rat.

To further understand the mechanistic pathway of AMX-GNPs after treatment in CP disease, we performed IHC staining of key inflammatory markers (NF-kB, IL-6). We observed a potential increment in immunopositive cells of NF-kB and IL-6 in diseased animal (Fig. 8H and Fig. S7, **Supplementary file**), due to development of chronic inflammation in pancreatic tissue. When we compared the free AMX treatment group to CP model group, we observed a potential reduction ($p < 0.05$*) in the % of IL-6 and NF-kB positive cells (Fig. S7B-C, **Supplementary file**). Notably, AMX-GNPs treatment significantly regulated expression of NF-kB and IL-6 compared to the disease group, additionally this effect was also higher than ($p < 0.01$**) AMX group (Fig. 8H and Fig. S7B-C, **Supplementary file**).

Subsequently, we evaluated IHC staining (Fig. 8H) of anti-inflammatory markers (IL-4), that suggested βGlu and AMX itself can be increased the % IL-4 immunopositive cells (Fig. 8H and Fig. S7D, **Supplementary file**) in pancreatic tissue most likely to immunomodulatory effect (macrophage reprogramming) of βGlu and AMX. While

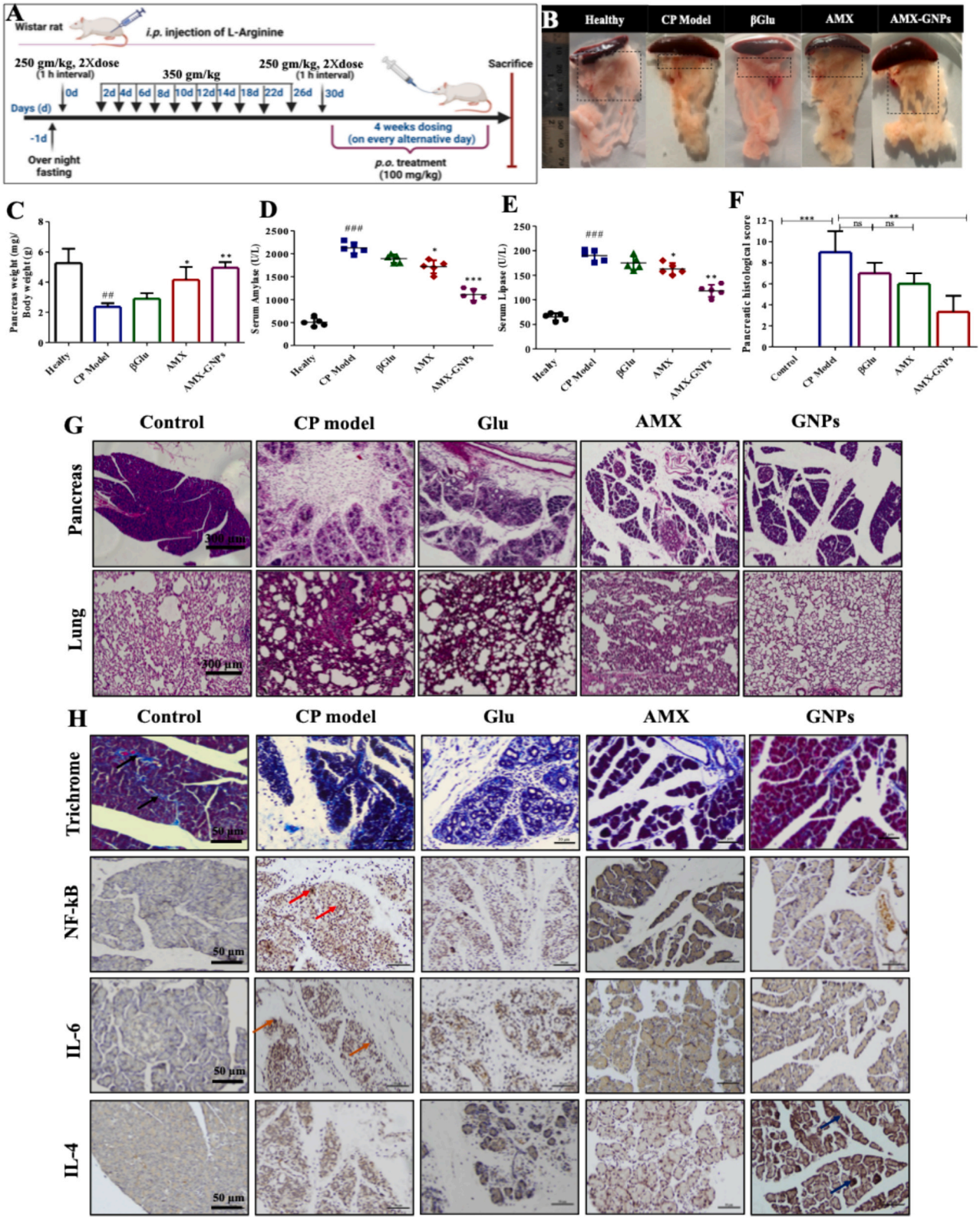

Fig. 8. Therapeutical efficacy of AMX-loaded βGlu-PLGA nanoparticles (AMX-GNPs) against Chronic pancreatitis (CP) (A). Schematic representation of experimental model and treatment timeline. (B). At the end of treatment schedule, pancreas was isolated, and images were captured for morphological assessment. (C) Graphs represent the pancreas to body weight ratio of every group. (D&E) Serum amylase and lipase level of treatment group, disease (CP) and healthy group (control) (F) Histopathological scoring of pancreatic tissue, scoring was done based on representative H&E staining. (G). Histopathological alterations in pancreas and lung were analysed by H&E staining (scale bar = 300 µm) (H). Anti-inflammatory effect of βGlu (β-Glucan), AMX, AMX-GNPs was evaluated using Masson's trichrome and IHC staining for NF-kβ, IL-6 and IL-4 expression in pancreatic tissue (scale bar = 50 µm). All graphs are presented as mean ± SEM (n = 3). Level of significance $p < 0.001$***, $p < 0.01$**, $p < 0.05$* & ns = $p > 0.05$.

tissue section AMX-GNPs treated CP rats exhibited notable ($p < 0.001$***) rise in IL-4 expression. Immunohistochemical analysis indicated AMX-GNPs treatment was showing potential effect on NF-kβ, IL-6 and IL-4 immunopositive cells against CP disease. This reduction might be attributed to the additive effects of AMX and β-Glucan, that overall, significantly inhibits the NF-κB, IL-6 and activate IL-4 expression (Fig. 8H and Fig. S7B-B, **Supplementary file**).

To further evaluate the immunomodulatory mechanism of AMX-GNPs in macrophage(Mϕ) reprograming in chronic inflammatory condition, we analysed NOS2 expression with immunofluorescence (ICF) staining in pancreatic tissue. The immunostaining results demonstrated a significant reduction in NOS2 (iNOS) expression in AMX-GNP treated group (results depicted in **Supplementary file**, Fig. S8), indicated that AMX-GNPs can modulate M1 Mϕ polarization through regulating NOS2 expression in inflammatory disease condition.

Subsequently, we performed a gene expression study on pancreatic tissues to determine the impact of AMX-GNPs (data presented in **Supplementary File**, Fig. S10) in CP animal, that showed potential effect on pro-inflammatory cytokines and Mϕ polarization at genetic level. For this, RT-PCR analysis was conducted to assess the mRNA levels of pro-inflammatory cytokine genes (IL-1β, TNF-α, and IL-6), as well as the M2 polarized Mϕ cell surface marker CD206 and the M1 polarized Mϕ cell surface marker NOS2 following oral treatment in diseased animals. The L-arginine induced chronic pancreatic injury caused significant difference ($p < 0.001$***) in mRNA level of IL-6, TNF-α, IL-1β, NOS2 and CD206 gene levels in disease group compared to healthy rats (Fig. S10A-E, **Supporting information**). The gene expression of M1 Mϕ associated pro-inflammatory cytokines genes were potentially reduced ($p < 0.05$*) in AMX treated group (Fig. S10A-C, **Supporting information**). In contrast βGlu treatment in CP rat, inhibits in M1 Mϕ associated gene and upregulate expression of M2 Mϕ associated gene (Fig. S10D-E, **Supporting information**). AMX-GNPs treatment potentially responsible for approximately two-fold reduction of IL-6, TNF-α, IL-1β, NOS2 gene expression and upregulated the M2 Mϕ associated gene CD206 (Fig. S10A-E, **Supporting information**). The significant effect of AMX-GNPs against the CP was found to be associated with core part of nanoparticles that contains AMX and β-Glucan both.

These all mechanistical studies revealed that AMX-GNPs effectively inhibit NF-κB signaling activity simultaneously reducing the expression of pro-inflammatory cytokines in CP. The recovery in chronic inflammation after AMX-GNPs treatment was also possible due to immunomodulatory effect, which inhibits the M1 Mϕ polarization and activation of M2 polarization of Mϕ. Further this parameter is responsible for decrease in inflammation and fibrosis in the pancreas, as well as reducing the levels of enzymes in the bloodstream, providing a promising treatment option for managing CP. Additional studies using immunohistochemical, immunofluorescence and gene expression analyses helped us to understand how AMX-GNPs reduces the chronic inflammation and contribute to their positive effects in treating chronic pancreatitis and understanding the potential mechanism of action.

4. Conclusion

In summary, we have designed AMX-GNPs for oral delivery of hydrophobic drug AMX with site-specific targeting via Dectin-1 receptor in AP and CP model. The β-Glucan surface modified PLGA nanoparticles are spherical in shape with size ranges around 100 ± 20 nm. It exhibited significant targeting ability for LPS activated macrophages (Mϕ), the intestinal M cell helps to uptake the GNPs due to specific binding for Dectin-1 receptor on these cells. Additionally, AMX-GNPs have potential to repolarize the pro-inflammatory Mϕ into anti-inflammatory Mϕ at target site. The GNPs can protect hydrophobic and acid sensitive drug molecules from harsh gastric environment and improve oral bioavailability. Moreover, the AMX-GNPs showed excellent anti-inflammatory effect by decreasing inflammatory cytokines and nitrite level in acute and chronic pancreatitis. The GNPs showed that they are biocompatible and safe for oral administration. The β-Glucan on outer surface of GNPs responsible for targeted and acid-resistant properties to protect the drug via oral route. The AMX-GNPs showed maximum reach at the targeted site by following ILS. Further AMX-GNPs effectively inhibits the NF-κB activation, pro-inflammatory cytokines release and modulate the Mϕ polarization due to AMX and β-Glucan. We also observed that AMX has significant anti-inflammatory potential but need to be given with carrier to upscale the bioavailability and further its specific effect. Overall, the combined effect of the AMX and GNPs potentially inhibited the inflammation and assisted to prevent the further progression of the pancreatitis in acute and chronic disease condition.

Collectively, our current study provides substantial evidence linking AMX-GNPs to NF-κB modulation by several downstream signaling molecules including cytokines such as IL-6, IL-1β and IL-4 with TNF-α, NOS-2 which exclusively follows NF-κB pathway [55–57]. Further, these markers have showed the effect on Mϕ reprogramming as well as influencing the NF-κB stimulation or downregulation. Further, this study explores partial mechanism of the upstream NF-κB pathway (e.g., IκBα phosphorylation, p65 nuclear translocation need to be explored) this would be our next goal to understand the direct involvement of the NF-κB upstream and downstream molecules in context to AMX-GNPs.

CRediT authorship contribution statement

Archana Karole: Writing – review & editing, Writing – original draft, Visualization, Validation, Methodology, Investigation, Formal analysis, Conceptualization. **Yirivinti Hayagreeva Dinakar:** Methodology. **Poonam Sagar:** Investigation. **Shabi Parvez:** Methodology. **Ravi Kumar:** Investigation. **Shyam Lal Mudavath:** Writing – review & editing, Writing – original draft, Supervision, Resources, Funding acquisition, Formal analysis, Conceptualization.

Declaration of competing interest

The authors declare that they have no known competing financial interests or personal relationships that could have appeared to influence the work reported in this paper.

Acknowledgements

All schematic illustrations were made using BioRender software. Archana Karole thanks Institute of Nano Science and Technology (INST), Mohali for providing the doctoral fellowship. This work is supported by the Government of India for funding under DST-SERB (EEQ/2020/000563), Indian Council of Medical Research, Govt. of India (IIRP-2023-3052) and Department of Biotechnology support to the School of Life Sciences, university of Hyderabad under the DBT-BUILDER program (BT/INF/22/SP41176/2020).

Appendix A. Supplementary data

Supplementary data to this article can be found online at https://doi.org/10.1016/j.cej.2025.163838.

Data availability

Data will be made available on request.

References

[1] G.J. Wang, C.F. Gao, D. Wei, C. Wang, S.Q. Ding, Acute pancreatitis: Etiology and common pathogenesis, World J. Gastroenterol. 15 (2009) 1427–1430, https://doi.org/10.3748/wjg.15.1427.

[2] T. Muniraj, H.R. Aslanian, J. Farrell, P.A. Jamidar, Chronic pancreatitis, a comprehensive review and update. Part i: Epidemiology, Etiology, Risk Factors, Genetics, Pathophysiology, and Clinical Features, Disease-a-Month 60 (2014) 530–550, https://doi.org/10.1016/j.disamonth.2014.11.002.

[3] Q. Zhang, S. Li, Y. Yu, Y. Zhu, R. Tong, A Mini-Review of Diagnostic and Therapeutic Nano-Tools for Pancreatitis, Int. J. Nanomedicine 17 (2022) 4367–4381, https://doi.org/10.2147/IJN.S385590.

[4] S. Tenner, J. Baillie, J. Dewitt, S.S. Vege, American College of Gastroenterology Guideline : Management of Acute Pancreatitis, Am J Gastroenterol 108 (2013) 1400–1415, https://doi.org/10.1038/ajg.2013.218.

[5] G.H. Sakorafas, A.G. Tsiotou, Etiology and Pathogenesis of Acute Pancreatitis: Current Concepts, J Clin Gastroenterol 30 (2000) 343–356, https://doi.org/10.1097/00004836-200006000-00002.

[6] B.W.M. Spanier, M.G.W. Dijkgraaf, M.J. Bruno, Epidemiology, aetiology and outcome of acute and chronic pancreatitis: An update, Best Pract Res Clin Gastroenterol 22 (2008) 45–63, https://doi.org/10.1016/j.bpg.2007.10.007.

[7] P. Lévy, E. Domínguez-Muñoz, C. Imrie, M. Löhr, P. Maisonneuve, Epidemiology of chronic pancreatitis: Burden of the disease and consequences, United European, Gastroenterol. J. 2 (2014) 345–354, https://doi.org/10.1177/2050640614548208.

[8] N.J. Schepers, O.J. Bakker, M.G. Besselink, U.A. Ali, T.L. Bollen, H.G. Gooszen, H. C. van Santvoort, M.J. Bruno, Impact of characteristics of organ failure and infected necrosis on mortality in necrotising pancreatitis, Gut 68 (2019) 1044–1051, https://doi.org/10.1136/gutjnl-2017-314657.

[9] Y. Song, S.H. Lee, Recent Treatment Strategies for Acute Pancreatitis, J. Clin. Med. 13 (2024), https://doi.org/10.3390/jcm13040978.

[10] L. Liu, Y. Zhang, X. Li, J. Deng, Microenvironment of pancreatic inflammation: calling for nanotechnology for diagnosis and treatment, J Nanobiotechnology 21 (2023) 1–22, https://doi.org/10.1186/s12951-023-02200-x.

[11] X. Zhong, G. Wang, F. Li, S. Fang, S. Zhou, A. Ishiwata, A.G. Tonevitsky, M. Shkurnikov, H. Cai, F. Ding, Immunomodulatory effect and biological significance of β-glucans, Pharmaceutics 15 (2023), https://doi.org/10.3390/pharmaceutics15061615.

[12] K. Lee, Y. Kwon, J. Hwang, Y. Choi, K. Kim, H.J. Koo, Y. Seo, H. Jeon, J. Choi, Synthesis and functionalization of β-glucan particles for the effective delivery of doxorubicin molecules, ACS Omega 4 (2019) 668–674, https://doi.org/10.1021/acsomega.8b02712.

[13] C. Fahlquist-Hagert, O. Sareila, S. Rosendahl, R. Holmdahl, Variants of beta-glucan polysaccharides downregulate autoimmune inflammation, Commun. Biol. 5 (2022), https://doi.org/10.1038/s42003-022-03376-y.

[14] H. Chen, Y. Sun, X. Xu, Q. Ye, Targeted delivery of methotrexate by modified yeast β-glucan nanoparticles for rheumatoid arthritis therapy, Carbohydr. Polym. 284 (2022) 119183, https://doi.org/10.1016/j.carbpol.2022.119183.

[15] X. Feng, Q. Xie, H. Xu, T. Zhang, X. Li, Y. Tian, H. Lan, L. Kong, Z. Zhang, Yeast microcapsule mediated natural products delivery for treating ulcerative colitis through anti-inflammatory and regulation of macrophage polarization, ACS Appl. Mater. Interfaces 14 (2022) 31085–31098, https://doi.org/10.1021/acsami.2c05642.

[16] G.D. Brown, J. Herre, D.L. Williams, J.A. Willment, A.S.J. Marshall, S. Gordon, Dectin-1 mediates the biological effects of beta-glucans, J. Exp. Med. 197 (2003) 1119–1124, https://doi.org/10.1084/jem.20021890.

[17] T. Phan Van, T. Huyen Ton Nu Bao, M. Leya, Z. Zhou, H. Jeong, C.W. Lim, B. Kim, Amlexanox attenuates LPS-induced neuroinflammatory responses in microglial cells via inhibition of NF–κB and STAT3 signaling pathways, Sci. Rep. 14 (2024) 1–16. doi: 10.1038/s41598-024-53235-5.

[18] X. Gan, M.W. Wilson, T.S. Beyett, B. Wen, D. Sun, S.D. Larsen, J.J.G. Tesmer, A. R. Saltiel, H.D. Showalter, Synthesis of deuterium-labelled amlexanox and its metabolic stability against mouse, rat, and human microsomes, J. Labelled Comp. Radiopharm. 62 (2019) 202–208, https://doi.org/10.1002/jlcr.3716.

[19] J.A. Loureiro, M.C. Pereira, PLGA based drug carrier and pharmaceutical applications: The most recent advances, Pharmaceutics 12 (2020) 1–5, https://doi.org/10.3390/pharmaceutics12090903.

[20] A. Karole, S. Parvez, R.S. Thakur, S.L. Mudavath, Effervescent based nano-gas carrier enhanced the bioavailability of poorly aqueous soluble drug: A comprehensive mechanistic understanding, J. Drug Deliv. Sci. Technol. 69 (2022) 103167, https://doi.org/10.1016/j.jddst.2022.103167.

[21] S. Parvez, A. Karole, S.L. Mudavath, Transport mechanism of hydroxy-propyl-beta-cyclodextrin modified solid lipid nanoparticles across human epithelial cells for the oral absorption of antileishmanial drugs, Biochim. Biophys. Acta (BBA) - General Subjects 1866 (2022) 130157, https://doi.org/10.1016/j.bbagen.2022.130157.

[22] M.C. Sheikh, S. Takagi, T. Yoshimura, H. Morita, Mechanistic studies of DCC/HOBt-mediated reaction of 3-phenylpropionic acid with benzyl alcohol and studies on the reactivities of “active ester” and the related derivatives with nucleophiles, Tetrahedron 66 (2010) 7272–7278, https://doi.org/10.1016/j.tet.2010.07.011.

[23] R.L. Mccall, R.W. Sirianni, PLGA Nanoparticles Formed by Single- or Double-emulsion with Vitamin E-, TPGS, J. Vis. Exp. 82 (2013) 51015, https://doi.org/10.3791/51015.

[24] A. Vyawahare, C. Jori, J. Kumar, N. Kanika, M. Fareed, N. Ali, K. Parida, R. Khan, A chlorogenic acid-conjugated nanomicelle attenuates disease severity in experimental arthritis, Biomater. Sci. 12 (2024) 3335–3344, https://doi.org/10.1039/d3bm02129g.

[25] K.S. Soppimath, T.M. Aminabhavi, A.R. Kulkarni, W.E. Rudzinski, Biodegradable polymeric nanoparticles as drug delivery devices, J. Controlled Release 70 (2001) 0168–3659, https://doi.org/10.1016/S0168-3659(00)00339-4.

[26] Y. Hayagreeva, A. Karole, S. Parvez, V. Jain, L. Mudavath, Folate receptor targeted NIR cleavable liposomal delivery system augment penetration and therapeutic efficacy in breast cancer, BBA - General Subjects 1867 (2023) 130396, https://doi.org/10.1016/j.bbagen.2023.130396.

[27] R. Prakash, A. Vyawahare, R. Sakla, N. Kumari, A. Kumar, M. Ansari, C. Jori, A. Waseem, A.J. Siddiqui, M.A. Khan, A.A.B. Robertson, NLRP3 inflammasome-targeting nanomicelles for preventing ischemia – reperfusion-induced inflammatory injury, ACS Nano 17 (2023) 8680–8693, https://doi.org/10.1021/acsnano.3c01760.

[28] S. Parvez, G. Yadagiri, A. Karole, O.P. Singh, A. Verma, Recuperating biopharmaceutical aspects of amphotericin B and paromomycin using a chitosan functionalized nanocarrier via oral route for enhanced anti-leishmanial activity, Sci. Rep. 10 (2020) 1–12, https://doi.org/10.3389/fcimb.2020.570573.

[29] B. Mamnoon, A.P. Mesquita Souza, T. Korzun, M.K. Baldwin, K.S. Sharma, O. Taratula, Y.T. Goo, P. Singh, V. Grigoriev, A. Lakhanpal, O.R. Taratula, ENT-1-targeted polymersomes to enhance the efficacy of methotrexate in choriocarcinoma treatment, Small Sci. (2025), https://doi.org/10.1002/smsc.202400361.

[30] A. Karole, D. Yirivinti Hayagreeva, P. Sagar, S.L. Mudavath, Self-assembled nano-micelles for oral delivery of luteolin utilizing intestinal lymphatic pathway targeting pancreatic cancer, Nanoscale (2024), https://doi.org/10.1039/d3nr06638j.

[31] Y.B. Miao, K.H. Chen, C.T. Chen, F.L. Mi, Y.J. Lin, Y. Chang, C.S. Chiang, J. T. Wang, K.J. Lin, H.W. Sung, A noninvasive gut-to-brain oral drug delivery system for treating brain tumors, Adv. Mater. 33 (2021), https://doi.org/10.1002/adma.202100701.

[32] M. Tashiro, C. Schäfer, H. Yao, S.A. Ernst, J.A. Williams, Arginine induced acute pancreatitis alters the actin cytoskeleton and increases heat shock protein expression in rat pancreatic acinar cells, Gut 49 (2001) 241–250, https://doi.org/10.1136/gut.49.2.241.

[33] P. Heygi, Z. Rakonczay, R. Sári, C. Góg, J. Lonovics, T. Takács, L. Czakó, L-arginine-induced experimental pancreatitis, World J. Gastroenterol. 10 (2004) 2003–2009, https://doi.org/10.3748/wjg.v10.i14.2003.

[34] H.K. Makadia, S.J. Siegel, Poly lactic-co-Glycolic Acid (PLGA) as biodegradable controlled drug delivery carrier, Polymers (basel) 3 (2011) 1377–1397, https://doi.org/10.3390/polym3031377.

[35] A.L.V. Zumaya, S. Rimpelová, M. Štějdířová, P. Ulbrich, J. Vilčáková, F. Hassouna, Antibody conjugated PLGA nanocarriers and superparmagnetic nanoparticles for targeted delivery of oxaliplatin to cells from colorectal carcinoma, Int. J. Mol Sci 23 (2022), https://doi.org/10.3390/ijms23031200.

[36] H. Chen, Y. Sun, X. Xu, Q. Ye, Targeted delivery of methotrexate by modified yeast β-glucan nanoparticles for rheumatoid arthritis therapy, Carbohydr. Polym. 284 (119183) (2022) 144–8617, https://doi.org/10.1016/j.carbpol.2022.119183.

[37] A. Abouzid, A.Y. Moustafa, N. Allcock, M. Najlah, A. Elhissi, C.W. Stanley, W. Ahmed, P. Seville, S.J. Crean, R.T. Forbes, M.A. Elsawy, Amlexanox-loaded nanoliposomes showing enhanced anti-inflammatory activity in cultured macrophages: a potential formulation for treatment of oral aphthous stomatitis, J. Drug Deliv. Sci. Technol. 79 (2023) 104052, https://doi.org/10.1016/j.jddst.2022.104052.

[38] S. Acar, Caffeic Acid Phenethyl Ester Loaded PLGA Nanoparticles: Effect of Various Process Parameters on Reaction Yield, Encapsulation Efficiency, and Particle Size, J. Nanomater 2015 (2015) 1–12, https://doi.org/10.1155/2015/341848.

[39] X. Zhan, J. Wan, G. Zhang, L. Song, F. Gui, Y. Zhang, Y. Li, J. Guo, R.K. Dawra, A. K. Saluja, A.N. Haddock, L. Zhang, Y. Bi, B. Ji, Elevated intracellular trypsin exacerbates acute pancreatitis and chronic pancreatitis in mice, Am. J. Physiol. Gastrointest. Liver Physiol. 316 (2019) G816–G825, https://doi.org/10.1152/ajpgi.00004.2019.

[40] C.K. Patel, T.K. Mukherjee, Biomolecular condensation of trypsin prevents autolysis and promotes Ca^{2+}-mediated activation of esterase activity, Biomacromolecules 25 (2024) 6082–6092, https://doi.org/10.1021/acs.biomac.4c00736.

[41] J. Glaubitz, S. Asgarbeik, R. Lange, H. Mazloum, H. Elsheikh, F.U. Weiss, M. Sendler, Immune response mechanisms in acute and chronic pancreatitis: strategies for therapeutic intervention, Front Immunol 14 (2023) 1–13, https://doi.org/10.3389/fimmu.2023.1279539.

[42] A. Al Madhoun, S. Kochumon, F. Al-rashed, S. Sindhu, R. Thomas, L. Miranda, F. Al-mulla, R. Ahmad, Dectin-1 as a potential inflammatory biomarker for metabolic inflammation in adipose tissue of individuals with obesity, Cells 11 (2022) 2879, https://doi.org/10.3390/cells11182879.

[43] C. Yunna, H. Mengru, W. Lei, C. Weidong, Macrophage M1/M2 polarization, Eur. J. Pharmacol. 877 (2020) 173090, https://doi.org/10.1016/j.ejphar.2020.173090.

[44] Y. Lin, Y. Chen, W. Feng, R. Hua, J. Zhang, Y. Huo, H. Jiang, B. Yin, X. Yang, Neddylation pathway alleviates chronic pancreatitis by reducing HIF1α-CCL5-dependent macrophage infiltration, Cell Death Dis. 12 (2021), https://doi.org/10.1038/s41419-021-03549-3.

[45] P.Y. Lin, K.H. Chen, Y.B. Miao, H.L. Chen, K.J. Lin, C.T. Chen, C.N. Yeh, Y. Chang, H.W. Sung, Phase-changeable nanoemulsions for oral delivery of a therapeutic peptide: toward targeting the pancreas for antidiabetic treatments using lymphatic transport, Adv. Funct. Mater. 29 (2019) 1–11, https://doi.org/10.1002/adfm.201809015.

[46] K.S. Kim, K. Suzuki, H. Cho, Y.S. Youn, Y.H. Bae, Oral nanoparticles exhibit specific high-efficiency intestinal uptake and lymphatic transport, ACS Nano 12 (2018) 8893–8900, https://doi.org/10.1021/acsnano.8b04315.

[47] A. Kumari, S.K. Yadav, S.C. Yadav, Biodegradable polymeric nanoparticles based drug delivery systems, Colloids Surf. B Biointerfaces 75 (2010) 1–18, https://doi.org/10.1016/j.colsurfb.2009.09.001.

[48] L. Johansson, L. Virkki, H. Anttila, H. Esselström, P. Tuomainen, T. Sontag-Strohm, Hydrolysis of β-glucan, Food Chem 97 (2006) 71–79, https://doi.org/10.1016/j.foodchem.2005.03.031.

[49] K.H. Chen, Y.B. Miao, C.Y. Shang, T.Y. Huang, Y.T. Yu, C.N. Yeh, H.L. Song, C. T. Chen, F.L. Mi, K.J. Lin, H.W. Sung, A bubble bursting-mediated oral drug delivery system that enables concurrent delivery of lipophilic and hydrophilic

chemotherapeutics for treating pancreatic tumors in rats, Biomaterials 255 (2020), https://doi.org/10.1016/j.biomaterials.2020.120157.
[50] J.M. Lee, H.S. Kim, M. Lee, H.S. Park, S. Kang, J.H. Nahm, J.S. Park, Association between pancreatic fibrosis and development of pancreoprivic diabetes after pancreaticoduodenectomy, Sci. Rep. 11 (2021) 1–8, https://doi.org/10.1038/s41598-021-02858-z.
[51] S.M. Reilly, S.H. Chiang, S.J. Decker, L. Chang, M. Uhm, M.J. Larsen, J.R. Rubin, J. Mowers, N.M. White, I. Hochberg, M. Downes, R.T. Yu, C. Liddle, R.M. Evans, D. Oh, P. Li, J.M. Olefsky, A.R. Saltiel, An inhibitor of the protein kinases TBK1 and IKK-ε improves obesity-related metabolic dysfunctions in mice, Nat. Med. 19 (2013) 313–321, https://doi.org/10.1038/nm.3082.
[52] J. Fujii, T. Osaki, Involvement of nitric oxide in protecting against radical species and autoregulation of M1-polarized macrophages through metabolic remodeling, Molecules 28 (2023), https://doi.org/10.3390/molecules28020814.
[53] G. Bögel, J. Murányi, B. Szokol, Z. Kukor, I. Móra, T. Kardon, L. Őrfi, A. Hrabák, Production of NOS2 and inflammatory cytokines is reduced by selected protein kinase inhibitors with partial repolarization of HL-60 derived and human blood macrophages, Heliyon 8 (2022) e08670, https://doi.org/10.1016/j.heliyon.2021.e08670.
[54] C.P. Delaney, K.F. Mcgeeney, P. Dervan, J.M. Fitzpatrick, Pancreatic atrophy: a new model using serial intra-peritoneal injections of l-arginine, Scand J. Gastroenterol. 28 (1993) 1086–1090, https://doi.org/10.3109/00365529309098314.
[55] T. Kolodecik, C. Shugrue, M. Ashat, E.C. Thrower, Risk factors for pancreatic cancer: Underlying mechanisms and potential targets, Front. Physiol. 4 JAN (2014), https://doi.org/10.3389/fphys.2013.00415.
[56] X. Jiang, Y.W. Zheng, S. Bao, H. Zhang, R. Chen, Q. Yao, L. Kou, Drug discovery and formulation development for acute pancreatitis, Drug Deliv. 27 (2020) 1562–1580, https://doi.org/10.1080/10717544.2020.1840665.
[57] T. Liu, L. Zhang, D. Joo, S.C. Sun, NF-κB signaling in inflammation, Signal Transduct. Target Ther. 2 (2017), https://doi.org/10.1038/sigtrans.2017.23.